Turkish Journal of Earth Sciences

Volume 33 | Number 2 Article 5

1-29-2024

# Evaluating the neotectonic activities of the Eastern Makran at the northern edge of the triple junction in southwest Pakistan

WASEEM KHAN
waseemmirwani@yahoo.com

KE ZHANG
eeszke@mail.sysu.edu.cn

HAO LIANG
liangh27@mail2.sysu.edu.cn

TÜBİTAK

Turkish Journal of Earth Sciences

http://journals.tubitak.gov.tr/earth/

Research Article

Turkish J Earth Sci
(2024) 33: 176-191

doi:10.55730/1300-0985.1905

# Evaluating the neotectonic activities of the Eastern Makran at the northern edge of the triple junction in southwest Pakistan

**Waseem KHAN*, Ke ZHANG, Hao LIANG**

Guangdong Provincial Key Laboratory of Geodynamics and Geohazards, School of Earth Sciences and Engineering, Sun Yat-Sen University, Zhuhai, China

**Received:** 18.03.2023 • **Accepted/Published Online:** 24.12.2023 • **Final Version:** 29.01.2024

**Abstract:** A number of five GIS-based indices, such as stream slope (*Ss*), surface roughness (*Sr*), asymmetric factor (*Af*), hypsometry integral (*Hi*), and stream-length gradient (*SL*), were summarised to examine the intensity of the index of tectonic activity (*IAT*) in 43 subbasins of Hingol Basin at the northern edge of the triple junction in southwest Pakistan. In addition, tectonic influences were identified by knickpoints spatial distribution and field surveys. The majority of the indices are consistent and display roughly the same classifications. The uncertain results have a less substantial impact on the obtained results in most of the 43 subbasins. Using these indices, the relative active tectonic index value (*IAT*) was calculated, revealing that tectonic activity is high along the north of the Awaran Fault and between the Nai Rud and Ornach-Nal faults, while other regions show moderate to low tectonic activity. Additionally, the knickpoint examinations showed higher tectonic intensity throughout the basin. The findings revealed a good relationship between the field surveys, past seismic analysis, and calculated geomorphic parameters.

**Key words:** Geomorphic parameters, knickpoints, neotectonic, Hingol Basin, Makran, Chaman Fault

## 1. Introduction

Tectonic geomorphology is the study of landforms caused by tectonic activity (Burbank and Anderson, 2012; Khan et al., 2022). The application of geomorphologic ideologies to solve tectonic complications is termed tectonic geomorphology (Keller and Pinter, 2002). The history, magnitude, and rate of these activities can be assessed by applying the geomorphic propositions (Keller and Pinter, 2002). A digital elevation model (DEM) is used to represent the quantitative investigation of the earth's surface (Summerfield, 1999). Geomorphic and topographic calculations are fundamentally examined on a DEM basis (Székely, 2001). Improved DEM and geospatial tools have significantly advanced geomorphic studies. Changes in tectonic activities alter the relative state of equilibrium in an active tectonic area (Keller and Pinter, 2002; Burbank and Anderson, 2012). Subsequently, the fluvial system is readjusted as per climate or tectonic changes (Burbank and Anderson, 2012). Finally, rivers record the tectonic processes of the geomorphologic evolution process. Thus, geomorphic indices are used to conduct (semi)quantitative morphotectonic analyses in order to determine the geomorphic characteristics and tectonics of a selected area (Brookfield, 1998; Keller and Pinter, 2002; Chen et al., 2003; Kobor and Roering, 2004; Hamdouni et al., 2008; Zygouri et al., 2015; Topal et al., 2016; Liu et al., 2020).

Over the recent past, huge advancements have taken place in the study of active tectonics in geomorphic basins. Bull and McFadden (1977) and Silva et al. (2003) applied the shape of the basin and asymmetric factor parameters to examine tectonic phenomena. Similarly, Hamdouni et al. (2008) conducted a study in Spain and calculated the relative tectonic activity using several geomorphic indices. Font et al. (2010) intensively studied an area in France and examined the relationship shared by channel gradient and hypsometry parameters to test neotectonic activities. Giaconia et al. (2012) used standard geomorphic indices to show the active tectonics of the Sierra Alhamilla. Joshi and Kotlia (2018) studied the lithology and tectonics of the landform in India on the basis of morphometric parameters. The aforementioned studies have shown that geomorphic indices are applicable for investigating geomorphic responses to tectonic activity.

Masson et al. (2004) found that the Arabian-Eurasian convergence led to extensive deformation at the Makran East-West Mountain ranges in Iran as well as in Pakistan. In the Hingol basin, there are two main tectonic lineaments. The Ornach-Nach Fault, which strikes NS, and a series of strikes running NNE-SSW with several smaller

* Correspondence: khanw@mail2.sysu.edu.cn

lineations make up the eastern lineament. They cause relief and drive gravitational and erosional processes. The NNE-SSW alignments cross several major rivers at high angles, mainly in the northeast, providing perfect geometries for studying the current neotectonic activities and their consequences on the rivers (Figure 1). Moreover, the homogenous climate and weak bedrock conditions, with no anthropogenic activities, create opportunities to examine tectonic-related studies (Haghipour et al., 2012; Smith et al., 2012; Haghipour and Burg, 2014). So, the goal of this research is to figure out how strong neotectonics are by using GIS-based geomorphologic parameters, field examinations, and past seismic evidence from Hingol Basin at the easternmost part of Makran at the northern edge of the triple junction in Pakistan.

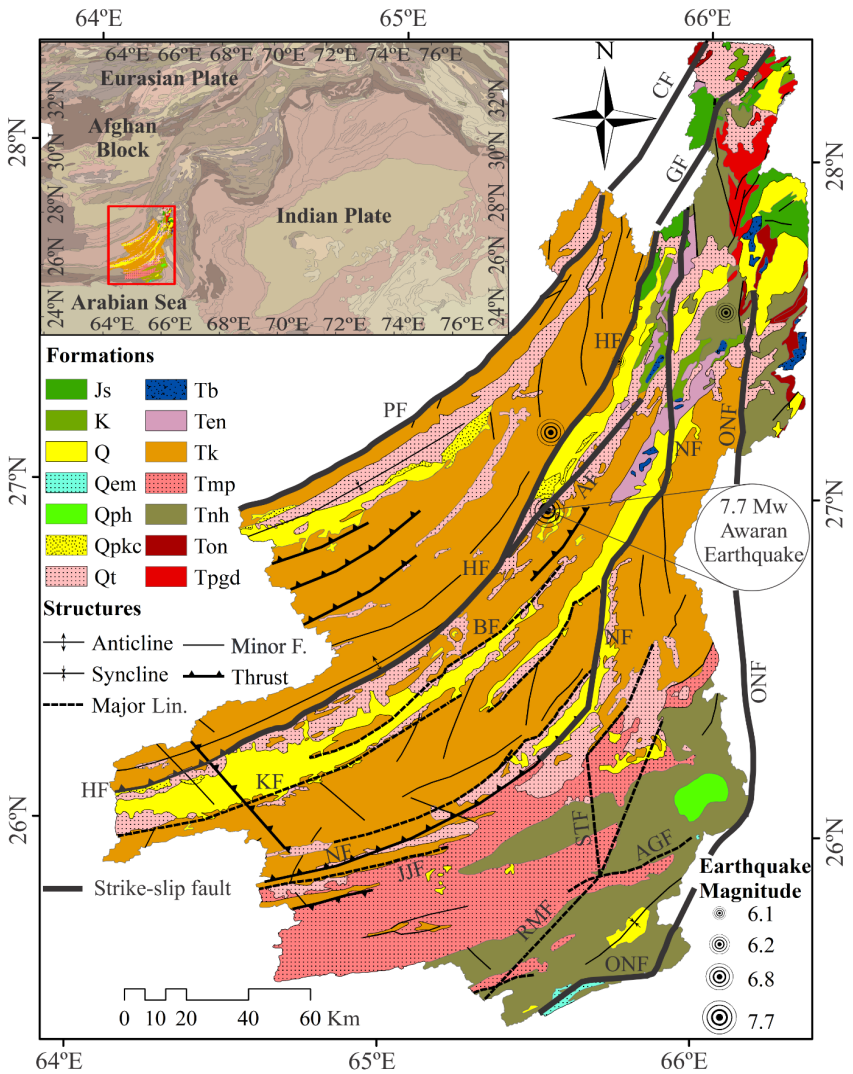


**Figure 1.** Geological map of the Hingol Basin, Pakistan. Js: Permian-Jurassic marine to continental sedimentary rocks at Indian Plate, K: Upper Jurassic-Late Oligocene shallow marine to continental deposits with lava flows in places and ophiolites at Indian Plate, Q: Recent sediments, Qem: Pliocene calcareous shale and marls, Qph: Quaternary shelly and reefoid limestone, conglomerate and sandstone, Qpkc: Quaternary conglomerate, Qt: Quaternary alluvial deposits, Tb: Palaeocene-Eocene Ophiolites, Ten: Jurassic-Oligocene sedimentary rocks at the Indian Plate, Tk: Oligocene-Early Miocene sandstone with interbedded shale, Tmp: Early Miocene mudstone and frequent thin sandstone, Tnh: Miocene-Pliocene mainly sandstones with conglomerate, shelly limestones, clayey shale, Ton: Eocene-Oligocene Limestone at Indian Plate, and Tpgd: Palaeocene-Eocene sandstone, conglomerate, limestone, shale and marls.Major Lin.: Major Lineations, Minor F.: Minor Faults, CF: Chaman Fault, GF: Ghazaband Fault, PF: Panjgur Fault, HF: Hoshab Fault, NF: Nai Rud Fault, JJF: Jhal Jhao Fault, KF: Kapp Fault, BF: Bazdad Fault, AF: Awaran Fault, ONF: Ornach Nal Fault, STF: Sistag Fault, RMF: Ras Malan Fault, AGF: Aghor Fault (after Khan et al., 2023b).

## 2. Regional framework

### 2.1. Geological and geographical background

The ephemeral Hingol River drains into the Arabian Sea in the Lasbela region (Delisle et al., 2002), which covers an area of approximately 27580.35 km$^2$ with a reach length of about 1647.8 km. The precipitation data from 2011 to 2020 (Harris et al., 2020) show an annual precipitation contrast of 140 to 298 mm with an increasing trend towards the north-northeast. The region experiences a climate ranging from arid to semiarid, characterized by an annual evaporation rate of about 1830 to 1930 mm. This rate typically exceeds the annual precipitation in the area (Kehl, 2009). The annual rainfall occurs between November and March, reaching its peak in January and February. However, glaciation is absent (Kehl, 2009). The Arabian Sea region receives two types of monsoon winds (Clemens and Prell, 2003; Haghipour and Burg, 2014). In summers, humid and warm monsoon winds blow from the southwest, while in winters, drier and weaker winds, in semiarid to arid environments, blow from the north-northeast.

The eastern boundary of the Hingol Basin is defined by the left-lateral strike-slip Ornach-Nal Fault, which originates in the southern region of the basin, where three tectonic plates—India, Eurasia, and Arabia—converge (Khan et al., 2023b) (Figure 1). This convergence of the three plates is generally expressed as the Markran triple junction in Pakistan (Khan et al., 2023a). The Ornach-Nal Fault follows a northerly direction from the Makran megathrust and then joins the Chaman Fault near Ornach village (Ruleman, 2005; Zhang et al., 2011). Hingol Basin comprises four major NE/SW trending faults from south to north: Nai Rud, Hoshab, Panjgur, and Siahan (not shown in the map) thrust faults (Figure 1). The region developed at the convergent margin of the Asian and Arabian plates, primarily from recycled sediments in the Cenozoic. These sediments were brought up by the older uplifted Indian-Asian collision zone (Harms et al., 1984; Fruehn et al., 1997). The detrital inputs from the Himalayas have been disconnected, making the Makran accretionary wedge self-maintained since the Lower Miocene (Schlüter et al., 2002; Mouchot et al., 2010). Moreover, half of the basin represents massive sedimentary beds in the Upper Oligocene to Lower Miocene Formation. Harms et al. (1982, 1984) argued that the northern parts (excluding the formations at the Indian Plate) were formed on the ocean floor, while the southern parts formed above the wedge in a slope-shelf environment. The northeastern part of the basin resembles Permian-Oligocene marine to continental sedimentary rocks of the Indian Plate and Palaeocene-Eocene ophiolitic rocks.

### 2.2. Seismic activities

The Ornach-Nal Fault is the southern extension of the Chaman Fault System, extending south from the arc-trench gap to the Arabian Sea. A number of four major earthquakes have been recorded with a maximum magnitude of 7.7 since 1990 in Hingol Basin (Figure 1) (source: USGS catalog). The occurrence of the 2013 Mw 7.7 earthquake in Awaran recently highlighted the continued deformation of the accretionary wedge faults underneath the subducting zone (Figure 1). The Nai-Rud (NF), Hoshab (HF), and Panjgur (PF) faults have been identified on the Makran accretionary prism (including Siahan fault but not shown here) (Figure 1). These faults in the Makran accretionary prism at the west are arcuate, with strikes bending northward, suggesting the effect of the Ornach-Nal Fault's left lateral shear. Shah et al. (2021) conducted a study across the Ornach-Nal Fault and computed a 15 mm/yr slip rate. The west side of the Ornach-Nal Fault was the epicentre of the 2013 earthquake, which propagated southwestward via the Awaran Fault (Figure 1). According to Barnhart et al. (2015), the strike-slip mechanism on the NE portion of the NNE-SSW fault converts to thrust when the fault's direction shifts farther toward E-W (Figure 1). Despite the fact that the 2013 mainshock was mostly a strike-slip occurrence, the aftershocks revealed considerable thrust activity west of Hingol Basin (Avouac et al., 2014). The eastern NE-SW-oriented segments (Figure 1) are expected to rupture in an oblique way according to this deformation model because the Chaman Fault is more likely to affect them. These faults were assigned a dip angle of 60° in the analysis undertaken by Zhou et al. (2016). The N-S compression causing active subduction is more likely to affect the western sections, which strike in an E-W direction (Figure 1). Geological and geophysical evidence indicates that faults in the western section of the basin exhibit a distinctive pure thrust characteristic, with an approximate dip of 30° (Crupa et al., 2017). By analysing InSAR data, the Siahan Fault (a similar fault at the north of Panjgur Fault with the same propagation as that of Panjgur Fault) in the northeast has a 2 mm/yr slip rate (Crupa et al., 2017). A comparable investigation conducted near the Kharan area by Huang et al. (2016) similarly revealed a 2 mm/yr slip rate. Thus, each fault in the accretionary wedge accommodates a 2 mm/yr compressional motion (Figure 1). According to Shah et al. (2021), with 30° thrust faulting at the west, a slip rate of 2.3 mm/yr was observed. However, the accretionary wedge's eastern fault segments have a resulting slip rate of 3.1 mm/yr (Shah, 2019). Thus, the new findings indicate more tectonic stress at the western E-W thrust segments. While the Awaran Fault, at the NNE of the Hoshab Fault (Figure 1), is the most active zone in Hingol Basin (Shah et al., 2021).

## 3. Methodology

Eight tiles of the Digital Elevation Model 30m were downloaded from https://dwtkns.com/srtm30m/. The

DEMs were processed and mosaicked in an ArcGIS 10.5 environment. A hydrology analyst tool was used to extract the Hingol Basin, and a total of 43 watershed subbasins were delineated within the Hingol Basin. Stream orders were defined using six numbers. In order to find the relative tectonic activity index (*IAT*) (Hamdouni et al., 2008), the geomorphic indices of the Hingol Basin were used. These included stream slope (*Ss*), surface roughness of the topography (*Sr*), stream length gradient (*SL*), hypsometry (*HI*), and asymmetry (*Af*). The *SL* index was calculated by the SLiX Toolbox (Piacentini et al., 2020) in an ArcGIS environment, and the rest of the parameters were analysed in the hydrology extension of the Spatial Analyst tool. In addition, knickpoints were identified using Point Pattern on Stream networks (PPS) within the MATLAB-based TopoToolbox environment for the river profile analysis of each subbasin. PPS comprises a set of MATLAB scripts that leverage TopoToolbox version 2 to delineate knickpoints (Schwanghart and Scherler, 2014; Schwanghart et al., 2021; Schwanghart, 2021). Thus, a combination of field examination and geological scenarios, along with GIS and remote sensing, were employed to quantitatively scrutinise the geomorphic progression and tectonic activities of the Hingol Basin.

## 4. Geomorphic parameters and results

### 4.1. Stream slope (Ss)

It is a representation of the dynamic equilibrium between stream transport capacity, substratum erodibility, and tectonic activities. The slope of the channel bed eventually rises to a point where the weathering materials and the product being removed are in balance (Huyghe et al., 2004; Lykoudi and Angelaki, 2004; Pánek, 2004). According to Kirby and Whipple (2001), the variations in the stream slope determine the rate of uplift resulting from tectonic activity. The increase in gradient indicates that the stream channel is adapting to the different rates of uplift, as the incision tries to reach equilibrium in the uplift of rocks.

The expression for this morphometric parameter is:

$$Ss = ((H_{max} - H_{min})/L_s \times 100, \quad (1)$$

where $H_{max}$ is the stream maximum altitude, $H_{min}$ is the stream minimum altitude, and $L_s$ is the stream length (Strahler, 1952). The $Ss$ values were grouped into 3 classes (Nourbakhsh, 2014) to determine the tectonic intensity, i.e. >3.1 (Class I), <3.1–1.18 (Class II), and <1.18 (Class III).

The $Ss$ values range from 0.30 (B36) to 4.05 (B41), with a mean value of 1.20 (Table 1). The $Ss$ of 2.33% belong to Class I, 39.53% belong to Class II, and 58.14% belong to Class III (Table 1; Figure 2a). This indicates moderate to low tectonic activity in the region.

### 4.2. Surface roughness (Sr)

A multitude of factors resulting from vertical articulation and the slope of the area contribute to the relief gradient and energy characteristics. The upsurge in erosion base and neotectonic motions are the primary contributors to relief energy (Pánek, 2004). Areas with significant uplift exhibit high surface roughness (Klinkenberg, 1992; Ascione et al., 2008). Surface roughness is calculated using the standard deviation of a surface's topography. In this study, $Sr$ of the basin surface is determined using the statistical toolkit of ArcGIS 10.5 (Nourbakhsh, 2014).

Classes were established to categorize $Sr$ values as follows: Class I (>280), Class II (280–170), and Class III(<170) (Piacentini et al., 2020). The calculated $Sr$ values range from 4.39 (B23) to 358.02 (B11), with a mean of 163.55. The results are divided into three categories: 6.98 percent for Class I, 39.53 percent for Class II, and 53.49 percent for Class III (Table 1; Figure 2b), indicating a range of tectonic activity from low to high in the area.

### 4.3. Asymmetric factor (Af)

The factor of asymmetry can be employed to assess tectonic activity at a basin's drainage size. It has a rather broad range of applications (Hare and Gardner, 1985; Keller and Pinter, 2002). The formula for the $Af$ indices is expressed by:

$$Af = (\frac{Ar}{At}) \times 100, \quad (2)$$

Here, $Ar$ denotes the area of key watercourse's right trunk and $At$ denotes the total area of the watershed basin.

The $Af$ ranges of 43 subbasins are presented in Table 1. Three classes are assigned to the range: Class I, <35 or >65; Class II, 57 to <65 or 35 to <43; and Class III 43 to <57 (e.g., Hare and Gardner, 1985; Keller and Pinter, 2002; Hamdouni et al., 2008). The mean $Af$ is 48.57, with values ranging from 15.68 (B10) to 84.42 (B43). Class I accounts for 27.91 percent, Class II for 30.23 percent, and Class III for 41.86 percent of the total (Table 1; Figure 2c), signifying moderate to low tectonic activities.

### 4.4. Stream length gradient (SL)

The parameter $SL$ reflects a structural balance between active tectonics (Keller and Pinter, 2002). Abrupt changes in channel slope are considered anomalous conditions and appear as "steps" along the river (knickpoints). Anomalous points can be associated with more erosion-resistant rocks, high-flow tributary junctions, and upstream erosion caused by a lower base level (Keller and Pinter, 2002). Discarding these possibilities, anomalous values may be due to tectonics and erodibility, for instance, in channel flows (Hack, 1973). The index is applied to assess active tectonics (Hamdouni et al., 2008) and is computed as follows:

$$SL = (\frac{\Delta H}{\Delta L}) \times L, \quad (3)$$

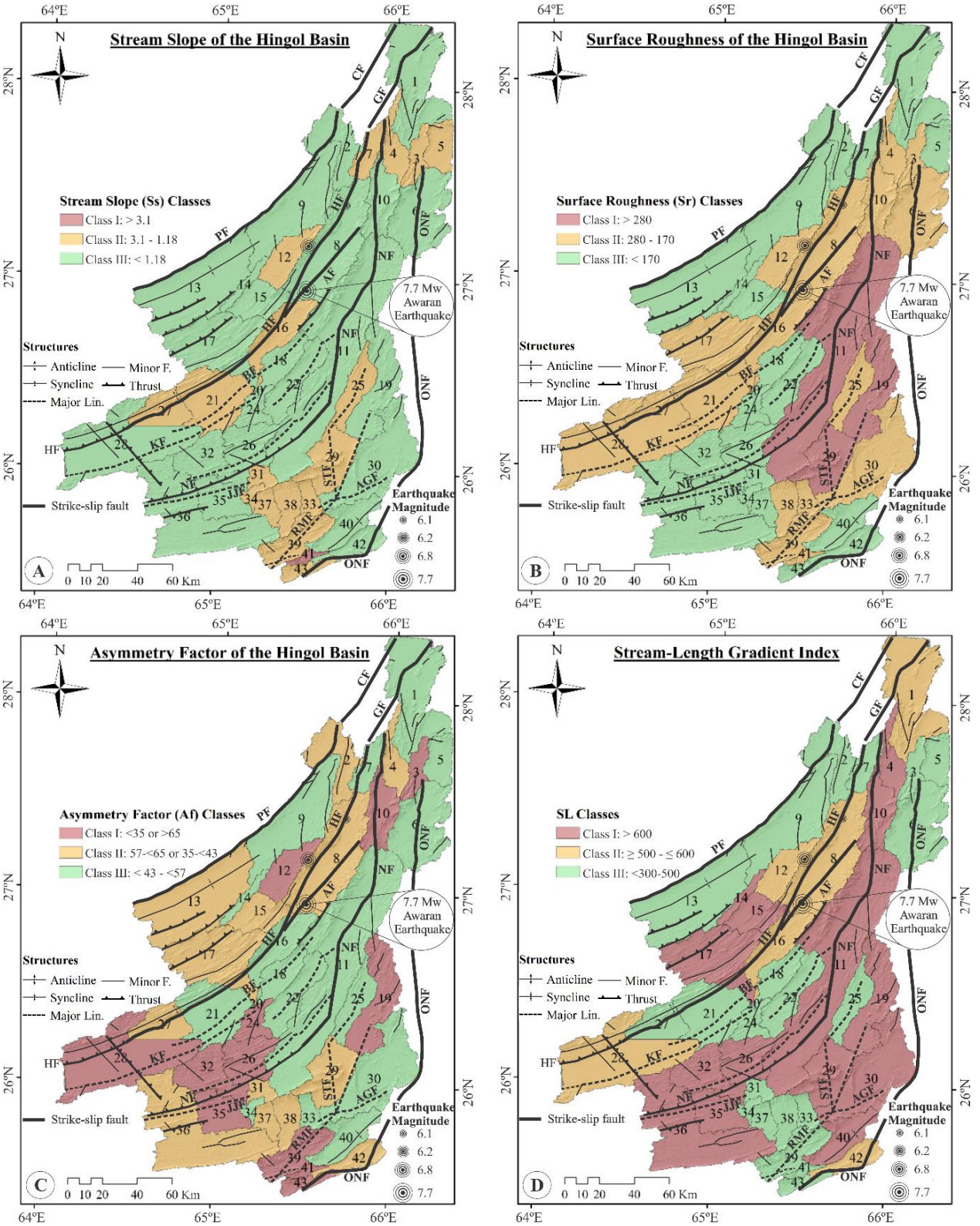


**Figure 2.** Demonstrating the five calculated geomorphologic parameters categorized into three classes: (a) stream slope, (b) surface roughness, (c) asymmetry factor, (d) stream length gradient. Note that all *Hi* classes fall in class 2 (not shown here). The numbers represent the subbasins. The captions of faults are the same as in Figure 1.

where $\frac{\Delta H}{\Delta L}$ is the stream reach's gradient. The difference in height of the reach is $\Delta H$, the reach's length is $\Delta L$, and the whole length of the stream from the upstream reach's midpoint of interest to the channel's greatest point is denoted by $L$.

Because $SL$ is reflective of variations in the slope of the stream, it is used to assess correlations between tectonic activities, the resistance of rocks, and topographic surfaces. While the stream runs through an uplifting area, $SL$ increases, and where the stream flows analogously to specific features, for instance, a basin formed by a strike-fault, $SL$ reduces (Keller and Pinter, 2002).

Higher $SL$ values imply that the highlands were not much eroded and reflect a young terrain, possibly caused by tectonic activities (Hamdouni et al., 2008). The intensity scales of *SL* are classified as Class I ≥600, Class II ≥500 to ≤600, and Class III ≤300–500 (Hamdouni et al., 2008).

For each subbasin, we determined the $SL$ standardised average value. The value varies between 181.36 (B34) and 3081.64 (B40). Table 1 shows how the data were divided into three classes: 32.56 percent belongs to Class I, 13.95 percent to Class II, and 48.84 percent to Class III. Due to their smallest basin sizes, 4.65% (B20 and B23) do not represent any $SL$ values (Figure 2d).

**Table 1.** The calculated five parameters, classes, and the Index of Active Tectonics (*IAT*) classes of the Hingol Basin. Here, *SS* represents stream slope, *Sr* represents surface roughness, *Af* represents asymmetric factor, *Hi* represents hypsometry integral, *SL* represents stream length gradient index, $\Sigma_C$ represents sum of the classes and *S/N* is referred to sum of classes divided number of classes.

| Basin | Ss | | Sr | | Af | | Hi | | SL | | IAT | | |
|---|---|---|---|---|---|---|---|---|---|---|---|---|---|
| | *Value* | *Class* | *Value* | *Class* | *Value* | *Class* | *Value* | *Class* | *Value* | *Class* | $\Sigma_C$ | *S/N* | *Class* |
| 1 | 0.44 | 3 | 135.73 | 3 | 48.02 | 3 | 0.4 | 2 | 500.05 | 2 | 13 | 2.6 | 4 |
| 2 | 0.67 | 3 | 101.87 | 3 | 38.8 | 2 | 0.32 | 2 | 389.56 | 3 | 13 | 2.6 | 4 |
| 3 | 1.84 | 2 | 216.84 | 2 | 73.91 | 1 | 0.21 | 2 | 273.43 | 3 | 10 | 2 | 3 |
| 4 | 1.24 | 2 | 195.56 | 2 | 58.53 | 2 | 0.18 | 2 | 677.1 | 1 | 9 | 1.8 | 2 |
| 5 | 2.18 | 2 | 164.68 | 3 | 54.93 | 3 | 0.18 | 2 | 226.4 | 3 | 13 | 2.6 | 4 |
| 6 | 0.87 | 3 | 180.11 | 2 | 44.28 | 3 | 0.19 | 2 | 491.99 | 3 | 13 | 2.6 | 4 |
| 7 | 1.33 | 2 | 116.02 | 3 | 54.36 | 3 | 0.28 | 2 | 310.64 | 3 | 13 | 2.6 | 4 |
| 8 | 0.81 | 3 | 249.3 | 2 | 41.75 | 2 | 0.32 | 2 | 548.98 | 2 | 11 | 2.2 | 3 |
| 9 | 0.5 | 3 | 163.75 | 3 | 48.39 | 3 | 0.33 | 2 | 259.01 | 3 | 14 | 2.8 | 4 |
| 10 | 0.9 | 3 | 186.85 | 2 | 15.68 | 1 | 0.31 | 2 | 927.53 | 1 | 9 | 1.8 | 2 |
| 11 | 0.49 | 3 | 358.02 | 1 | 46.44 | 3 | 0.26 | 2 | 896.56 | 1 | 10 | 2 | 3 |
| 12 | 1.85 | 2 | 209.83 | 2 | 17.93 | 1 | 0.24 | 2 | 582.18 | 2 | 9 | 1.8 | 2 |
| 13 | 0.36 | 3 | 91.75 | 3 | 41.21 | 2 | 0.24 | 2 | 343 | 3 | 13 | 2.6 | 4 |
| 14 | 0.72 | 3 | 71.86 | 3 | 46.47 | 3 | 0.35 | 2 | 640 | 1 | 12 | 2.4 | 3 |
| 15 | 0.77 | 3 | 128.12 | 3 | 57.63 | 2 | 0.34 | 2 | 817.35 | 1 | 11 | 2.2 | 3 |
| 16 | 1.31 | 2 | 225.64 | 2 | 56.8 | 3 | 0.31 | 2 | 585.35 | 2 | 11 | 2.2 | 3 |
| 17 | 0.85 | 3 | 195.9 | 2 | 37.6 | 2 | 0.41 | 2 | 1054.8 | 1 | 10 | 2 | 3 |
| 18 | 1.12 | 3 | 125.89 | 3 | 46.89 | 3 | 0.2 | 2 | 290.52 | 3 | 14 | 2.8 | 4 |
| 19 | 1.13 | 3 | 298.39 | 1 | 25.04 | 1 | 0.3 | 2 | 774.86 | 1 | 8 | 1.6 | 2 |
| 20 | 0.74 | 3 | 9 | 3 | 46.22 | 3 | 0.31 | 2 | - | - | 11 | 2.8 | 4 |
| 21 | 1.45 | 2 | 217.36 | 2 | 56.38 | 3 | 0.2 | 2 | 394.45 | 3 | 12 | 2.4 | 3 |
| 22 | 0.76 | 3 | 115.93 | 3 | 43.01 | 3 | 0.21 | 2 | 389.4 | 3 | 14 | 2.8 | 4 |
| 23 | 0.94 | 3 | 4.39 | 3 | 46.93 | 3 | 0.31 | 2 | - | - | 11 | 2.8 | 4 |
| 24 | 0.71 | 3 | 85.05 | 3 | 72.56 | 1 | 0.34 | 2 | 395.24 | 3 | 12 | 2.4 | 3 |
| 25 | 1.8 | 2 | 188.3 | 2 | 56.1 | 3 | 0.16 | 2 | 405.72 | 3 | 12 | 2.4 | 3 |
| 26 | 0.48 | 3 | 138.43 | 3 | 67.48 | 1 | 0.34 | 2 | 997.09 | 1 | 10 | 2 | 3 |
| 27 | 1.63 | 2 | 233.25 | 2 | 38.66 | 2 | 0.24 | 2 | 467.33 | 3 | 11 | 2.2 | 3 |
| 28 | 0.71 | 3 | 177.91 | 2 | 32.81 | 1 | 0.13 | 2 | 594.58 | 2 | 10 | 2 | 3 |
| 29 | 1.32 | 2 | 287.81 | 1 | 59.88 | 2 | 0.23 | 2 | 848.33 | 1 | 8 | 1.6 | 2 |
| 30 | 0.59 | 3 | 182.97 | 2 | 43.55 | 3 | 0.34 | 2 | 920.41 | 1 | 11 | 2.2 | 3 |
| 31 | 1.74 | 2 | 80.76 | 3 | 62.17 | 2 | 0.19 | 2 | 421.58 | 3 | 12 | 2.4 | 3 |
| 32 | 0.82 | 3 | 157.6 | 3 | 25.24 | 1 | 0.47 | 2 | 845.39 | 1 | 10 | 2 | 3 |
| 33 | 2.91 | 2 | 216.6 | 2 | 43.03 | 3 | 0.14 | 2 | 190.13 | 3 | 12 | 2.4 | 3 |
| 34 | 1.78 | 2 | 68.52 | 3 | 44.09 | 3 | 0.19 | 2 | 181.36 | 3 | 13 | 2.6 | 4 |
| 35 | 0.77 | 3 | 90.09 | 3 | 68.92 | 1 | 0.32 | 2 | 604.39 | 1 | 10 | 2 | 3 |
| 36 | 0.3 | 3 | 154.54 | 3 | 58.91 | 2 | 0.23 | 2 | 890.16 | 1 | 11 | 2.2 | 3 |
| 37 | 1.33 | 2 | 96.68 | 3 | 63.73 | 2 | 0.16 | 2 | 388.39 | 3 | 12 | 2.4 | 3 |
| 38 | 2.16 | 2 | 188.15 | 2 | 60.72 | 2 | 0.14 | 2 | 239.39 | 3 | 11 | 2.2 | 3 |
| 39 | 1.91 | 2 | 247.91 | 2 | 21.46 | 1 | 0.23 | 2 | 467.41 | 3 | 10 | 2 | 3 |
| 40 | 1.15 | 3 | 145.96 | 3 | 44 | 3 | 0.32 | 2 | 3081.6 | 1 | 12 | 2.4 | 3 |
| 41 | 4.05 | 1 | 245.45 | 2 | 33.35 | 1 | 0.23 | 2 | 198.47 | 3 | 9 | 1.8 | 2 |
| 42 | 0.67 | 3 | 141.22 | 3 | 60.08 | 2 | 0.25 | 2 | 501.45 | 2 | 12 | 2.4 | 3 |
| 43 | 1.55 | 2 | 142.72 | 3 | 84.42 | 1 | 0.14 | 2 | 201.07 | 3 | 11 | 2.2 | 3 |
| **Mean** | **1.2** | **2.6** | **163.55** | **2.47** | **48.57** | **2.14** | **0.26** | **2** | **590.55** | **2.17** | **11.23** | **2.3** | **3.14** |
| **Min** | 0.3 | 1 | 4.39 | 1 | 15.68 | 1 | 0.13 | 2 | 181.36 | 1 | 8 | 1.6 | 2 |
| **Max** | 4.05 | 3 | 358.02 | 3 | 84.42 | 3 | 0.47 | 2 | 3081.6 | 3 | 14 | 2.8 | 4 |

### 4.5. Hypsometry integral (Hi)

The elevation dispersion in a specific geographic region is reflected by $Hi$ (Strahler, 1952). It is demarcated by an area lower than the curve of hypsometry. It indicates the volume of uneroded regions in the basin. This index is calculated using this simple calculation as follows (Pike and Wilson, 1971; Mayer, 1990; Keller and Pinter, 2002):

$$Hi = (H_{mean} - H_{min})/(H_{max} - H_{min}), \quad (4)$$

where $H_{mean}, H_{min}, H_{max}$, represent the mean, minimum, and maximum elevations, respectively.

Three values may be easily retrieved from the research area's DEMs. The $Hi$ ratios vary between 0 and 1. The range of 0 corresponds to heavily eroded and inactive tectonic provinces, while 1 corresponds to young and less eroded landforms, which are associated with tectonic activities (Keller and Pinter, 2002).

A higher index is associated with recent active tectonics, whereas lower ratios are associated with mature landforms that are more degraded and less influenced by the latest tectonic activities. A high $Hi$ is often convex, and its value is usually >0.5. The stage of maturity is defined by convexity to concavity, with $Hi$ ranging from 0.4 to 0.5. Lastly, the lower range (0.4) is considered concave (Hamdouni et al., 2008). The $Hi$ curves of the studied results are shown in Figure 3. The calculated $Hi$ values vary from 0.13 (B28) to 0.47 (B32), with a mean value of 0.26. The results suggest that all of the subbasins are classified as Class II, indicating convex to concave stage of maturity with moderate active tectonics (Table 1).

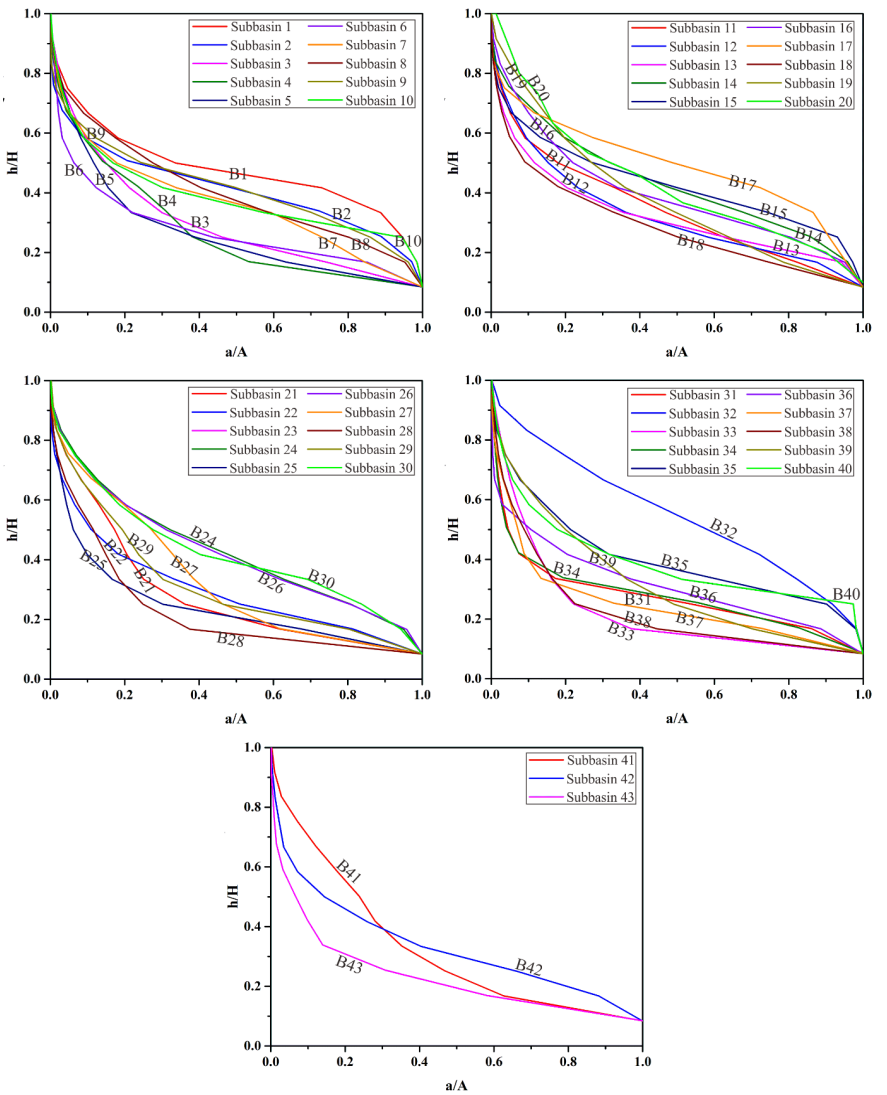


**Figure 3.** Calculated hypsometric curves of the Hingol Basin. The subbasins with young stages are 1, 2, 10, 15, 17, 30, and 32, and those with mature stages are 6, 8, 9, 12, 13, 14, 16, 24, 26, 31, 35, 36, 40, and 42, while those with old stages are 3, 4, 5, 7, 11, 18, 19, 21, 22, 25, 27, 28, 29, 33, 34, 37, 38, 39, 41, and 43.

**4.6. Index of tectonic activity (IAT)**

The five geomorphologic parameters were calculated to find out the index of *IAT*, as described by Hamdouni et al. (2008). This index is defined as the sum of the values and mean of the geomorphologic indices (Habibi and Gharibreza, 2015).

$$IAT = S/N \quad (5)$$

The summation of indices is denoted by 'S,' with the total number of indices expressed as 'N.' To quantify the intensity of active tectonics, the *IAT* index values are categorized into four distinct classes (Table 2) (Font et al., 2010). The *IAT* ratios vary from 1.6 to 2.8, with a mean of 2.3 (Table 1), indicating 13.95 percent of Class II, 58.14 percent of Class III, 27.91 percent of Class IV, and no *IAT* values in Class I. The classes indicate moderate to low tectonics in the studied region. Table 1 and Figure 4 display the *IAT* classes of the 43 subbasins.

**4.7. Knickpoints spatial distribution**

The form of river profiles in a bedrock channel tends to approach a graded profile by regulating upstream release and load transport (Gilbert, 1877; Mackin, 1948). To describe graded river profiles, a phenomenal affiliation with the slope of the channel and the related upstream watershed region can be employed (Flint, 1974; Howard, 1983). It is calculated by:

$$S = K_s A^{\theta}. \quad (6)$$

Here, the steepness of the channel index is $K_s = (U/K)^{1/n}$, and the concavity is $\theta = m/n$. The steady-state rock uplift/erosion ($E$) degree is $U$. While the erosion efficacy reflecting a collection of aspects is $K$, which governs channel erosion, with a ratio of 0.5 in a typical basin, there are positive constants $m$ and $n$ (Tucker and Whipple, 2002; Whipple et al., 2013).

The $\theta$ and $K_s$ may be calculated using channel slope (linear regression) vs. area of drainage (log-log plot) (Kirby and Whipple, 2001; Wobus et al., 2006). However, little changes and/or uncertainties can cause substantial changes in $K_s$. Hence, linking catchments of several sizes and shapes $K_{sn}$ (normalised) and a *ref* concavity is critical (Wobus et al., 2006).

$$S = K_{sn} A^{-\theta_{ref}} \quad (7)$$

For steady-state channels, the *ref* is the concavity parameter mean for entire channels in a basin, which falls between a given range of $0.4 \leq \theta \geq 0.6$ (Kirby and Whipple, 2001; Wobus et al., 2006). The $\theta_{ref}$ can also be computed using least scatter χ-elevation analysis (Tucker and Whipple, 2002; Whipple et al., 2013) and linear fitting of channel profiles (Goren et al., 2014; Jaiswara et al., 2019). The $K_{sn}$ may be determined by regressing a specified upstream and downstream border data range, as well as the whole channel (Snyder et al., 2003).

A total of 209 knickpoints were generated in Hingol Basin (Appendix; Figure 5a). The Hingol drainage basin's main channel and tributaries both have sudden variations in the gradient of their longitudinal profiles, indicating solitary knickpoints. Some of the knickpoints' steps are a few metres long, while numerous demonstrate convex parts with varying amplitudes, slopes, and locations. The causes responsible for the origin of most of these knickpoints were recognised and categorized into two types, as explained below. These knickpoints were separated into migratory (slope break) and fixed (vertical step) types based on their origin. The average height of knickpoints is 37.34 m, with values ranging from 20.02 to 243.91 m. Further, the knickpoint heights and elevations were grouped into five classes due to the large number of data points and are present in Table 3. Among these five classes, 119 (56.94%) knickpoints belong to the range of 20.02 to 30.0 m height; 54 (25.84%) knickpoints belong to the range of 30.00 to 45.64 m height; 22 (10.53%) knickpoints belong to the range of 45.64 to 71.89 m height; 9 (4.31%) knickpoints belong to the range of 71.89 to 136.05 m height; and 5 (2.39%) knickpoints belong to the range of 136.05 to 243.91 m height. The 40.19% of obtained values belong to fixed or vertical-step knickpoints denoting limited tectonic significance, while 59.81% belong to migratory or slope-break knickpoints indicating significant tectonic movements, for instance, fault initiation and/or increased fault slip (Figure 5b; Appendix).

**Table 2.** Detailed class ranges of index of active tectonics (Hamdouni et al., 2008).

| Class | Range | Tectonic activity |
|---|---|---|
| 1 | ≤1.0 to <1.5 | Extreme |
| 2 | ≤1.5 to <2.0 | High |
| 3 | ≤2.0 to <2.5 | Moderate |
| 4 | ≤2.5 to ≤3.0 | Low |

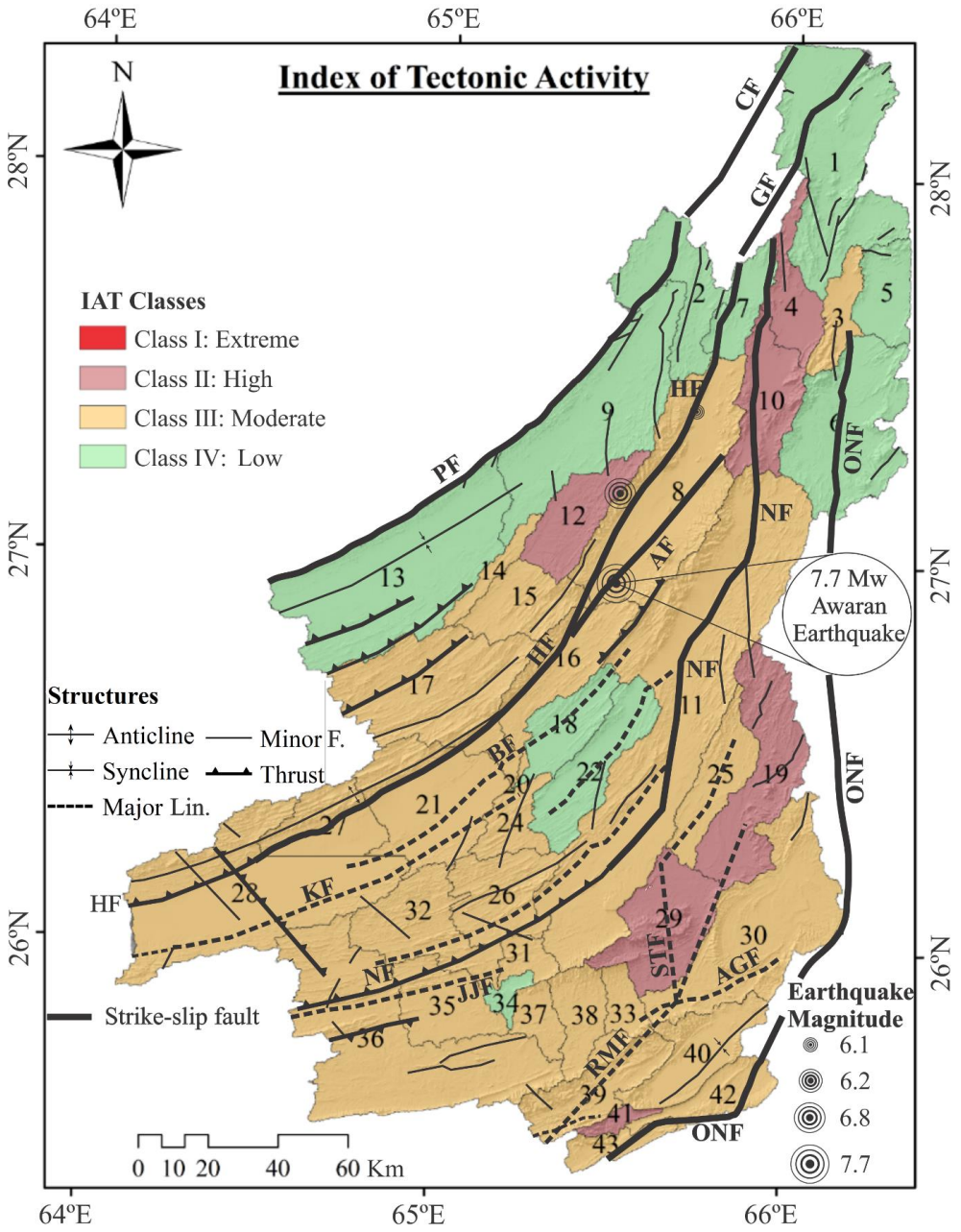


**Figure 4.** Illustration of nominal classes for IAT Classes in the Hingol Basin map. Note that no basin with Class 1 exists among the 43 subbasins. The numbers represent the subbasins. The captions of the faults are the same as in Figure 1.

## 5. Discussion

### 5.1. Neotectonic assessment by summarized IAT

The subbasins 12 at the north of the Awaran Fault (an eastern extension of the Hoshab Fault), subbasins 4 and 10 northeast of the Nai Rud Fault, subbasins 19 and 29 between the Nai Rud Fault and the Ornach-Nal Fault, and subbasin 41 at the southwestern part of the Ornach-Nal Fault have high *IAT* values. Structures in the Hingol Basin show that the Arabian and Indian plates are moving from north to south, east to west, and north to south-west in relation to the Eurasian Plate.

In most subbasins, geomorphic indices show *IAT* Classes II and III within most of the southern portions, indicating high to moderate tectonic activity. The northern areas, on the other hand, have *IAT* Class IV and are thought to have less tectonic activity. This can also

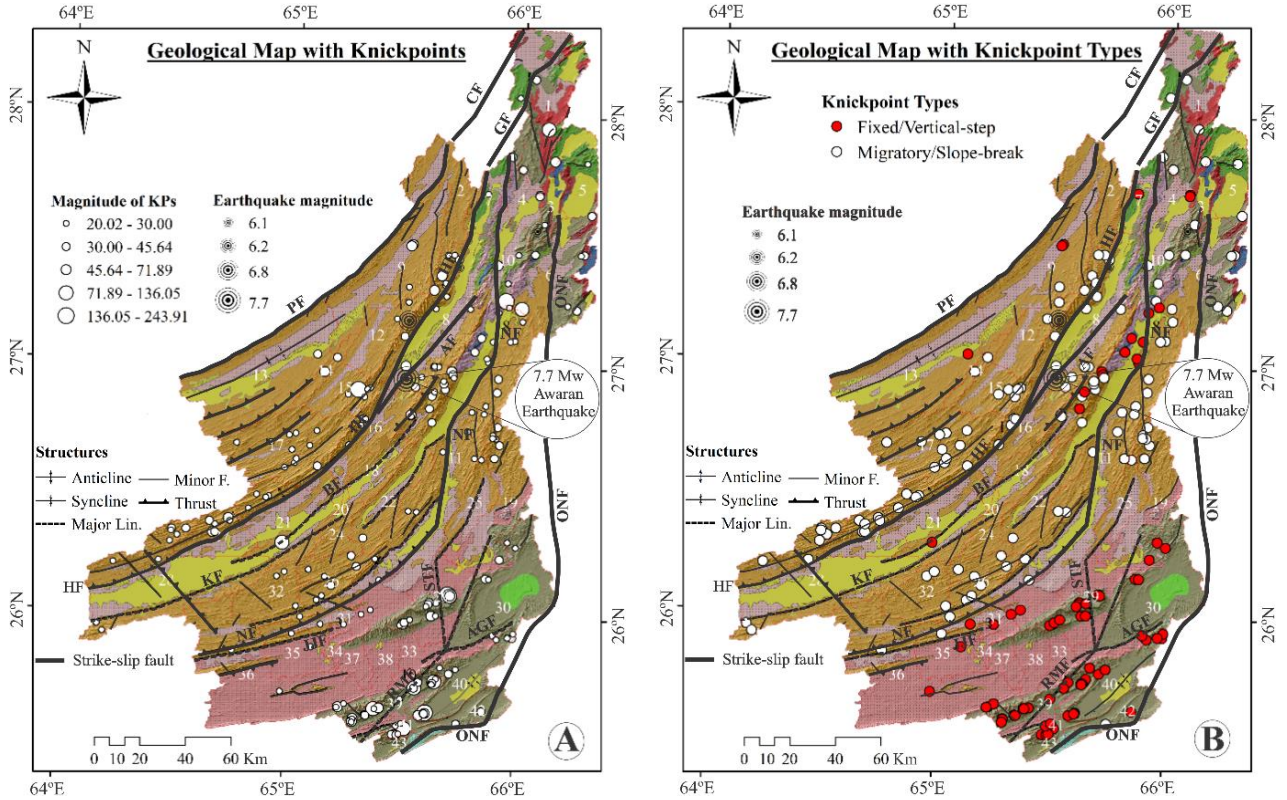


**Figure 5.** The geological map showing: (A) the intensities of knickpoint throughout the Basin and (B) the types of knickpoints in the basin. The numbers in white represent the basin number and numbers in black represent associated faults. Other legends are the same as in Figure 1.

**Table 3.** The summarized ranges of knickpoints and elevations extracted from the Hingol Basin (for detailed knickpoints data, the readers are referred to Appendix).

| S. No | KPs height (m) | Numbers | % of KPs | KPs elevation (m) | Number | % of elevation |
|---|---|---|---|---|---|---|
| 1 | 20.02 to <30.00 | 119 | 56.9378 | 68 to 373 | 47 | 22.48803828 |
| 2 | 30.00 to <45.64 | 54 | 25.83732 | 374 to 675 | 35 | 16.74641148 |
| 3 | 45.64 to <71.89 | 22 | 10.52632 | 676 to 982 | 48 | 22.96650718 |
| 4 | 71.89 to <136.05 | 9 | 4.30622 | 983 to 1248 | 46 | 22.00956938 |
| 5 | 136.05 to 243.91 | 5 | 2.392344 | 1248 to 1786 | 33 | 15.78947368 |
| Total | | **209** | **100** | | **209** | **100** |

be explained by the predominance of clastic rocks in the subbasins in the northern parts due to the vast region covered by the Panjgur Formation; as a result, weathering and erosion occur at about the same rates and grades. Thus, the *IAT* is lithological-related rather than tectonic-related. Accordingly, with an exception caused by the existence of diverse rock types rather than clastic in subbasin 1, the ratio of the valley length to its width remains approximately the same, creating a big uncertainty in the *IAT* calculation.

For much of the along-strike and its surroundings, high (Class II) *IAT* values suggest a complicated tectonic framework and significant erosion due to decreased plant cover, greater incision, and extremely steep sections (Figure 4). Low *IAT* values (Class IV) are found primarily in B1, B5, B6 (Indian Block), B2, B9, B13 (south of the Siahan Fault), and B18, B22, and B34 (adjacent to the Awaran Fault) (Figures 1 and 4). This is probably due to reduced erosive conditions and alluvial deposits; thus, the bulk of geomorphic indices reflect minimal tectonic activity.

**5.2. IAT assessment by lithological contrasts and field evidence**

The following factors are responsible for the prevalence of moderate to low tectonic activity in the Hingol Basin: (1) With the exception of the northern subbasins B1, B3, B4, B5, B6, B7, and B10, most of the exposed rocks in the 43 subbasins are clastics. These rocks include ophiolites, lava flows, calcareous shale, and limestone sandstone beds. Despite the fact that these rocks are exposed in B1, B3, B4, B5, B6, B7, and B10, their covering area is quite limited, extending exclusively along the Indian Plate's Kirthar Fold belt (Figures 1 and 5). As a result, the clastic rocks covering the largest areas of the Hingol basin have a significant influence on geomorphological indices, as well as the carbonate rocks in B1 and the southernmost parts of the Hingol Basin. (2) Because the maximum area falls within the region of the low folded zone and is subjected to the same tectonic stresses over time. (3) The form, size, and arrangement of the valleys are nearly identical in the southern parts of the Hingol basin due to the predominance of clastic rocks and the similar climatic conditions in terms of yearly rainfall and temperature.

The five geomorphic indices are summarised among the three primary classes of Hamdouni et al.'s (2008) (Table 1). This can be attributed to the following outcomes: (1) Layers of solid sandstone, mudstone, and conglomerate can have a local effect on the shape, width, and depth of valleys (Figure 6). Because of this, different results are found in different places within the same subbasins. (2) The amount of exposed rock can affect the symmetry of valleys. For example, when exposed rocks on both sides of a valley run along strike, the dipping amount varies on both sides of the exposed rocks, resulting in the asymmetry of the valley. (3) Within specific subbasins, soft and thick sandstone, shale, mudstone, and conglomerate layers, particularly in the Panjgur Formation and the southern sections, have flat or gently sloping regions (Figure 6); as a result, the obtained values vary from other indices. (4) The index of *SL* varies greatly, with the majority falling within Class III. This suggests minimal active tectonics. The dominance of clastic rock in the Hingol Basin is probably to blame for the roughly equal degrees of weathering and erosion.

**5.3. Neotectonic assessment by knickpoints distribution**

**5.3.1 Fault-related knickpoints**

The positions of knickpoints along the major fault zones in the Eastern Makran show a strong association between tectonic activities and stream gradient variation features. This perfect match of knickpoints and faults (Figure 5) shows that the river profile was adjusted to basement blocks with varying vertical displacements. As a result, differential vertical displacement or rock strength reduction that results in minimum resistivity is what causes the knickpoints seen along strikes.

**5.3.2. Lithological contrasts-related knickpoints**

The lithology in the Hingol Basin is thought to be rather homogeneous, so the variation in rock resistivity was skipped as a factor of knickpoint generation. The low strength of rocks along strikes is not thought to be lithological knickpoint sources, which are ascribed to fault-related knickpoints (Figure 5). The diverse geology responds differently to river erosion and weathering in sedimentary layer outcroppings on the NNW Indian Plate in the Hingol basin, resulting in knickpoint generation.

The longitudinal characteristics of the streams divided into three zones showed a significant lithological influence. The first zone, established on the Mesozoic to Cenozoic sequences of the sedimentary covers, is found on the Indian margin at the NNE (Figures 1 and 5). The series is mostly limestone, with varying amounts of arenaceous sequences. The sequences of NNE Indian Margin limestone and dolomitic rock types are more resistant to erosion than the sandstone flysch formation in Inner and Coastal Makran, resulting in a dramatic cliff in this part of the basin. The second zone is found in the Inner Makran (Makran Flysch) and largely consists of the Oligocene to Miocene Panjgur Formation (Kassi et al., 2015). While the third zone, known as the Coastal Makran, evolved on the southern sections with Miocene to Recent sedimentary coverings (Hunting Survey Corporation, 1960). The second and third zones (Inner and Coastal Makran, respectively) are both dominated by lithological control. After passing the same lithological contacts, the tributary streams discharge into the strikes. On this lithotype, knickpoints often form in these parts of the basin. The lithologic connections follow the direction of the main strikes in the region.

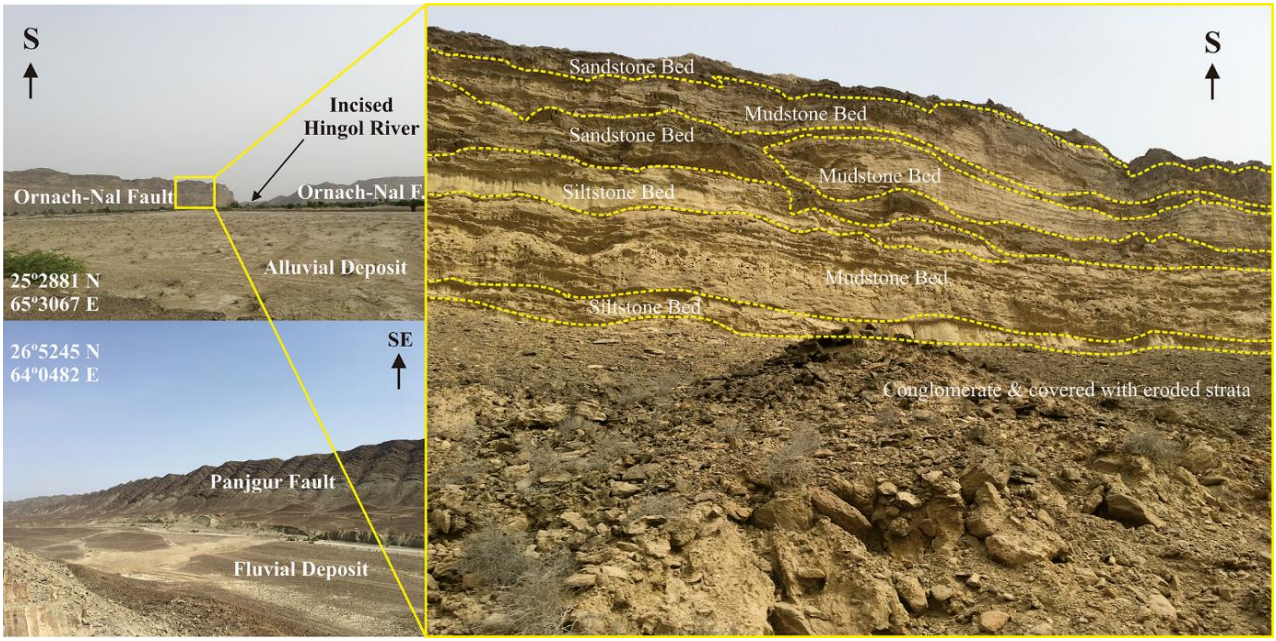


**Figure 6.** Field photos illustrating Ornach-Nal Fault (left-up), Panjgur Fault (left-down), and bedding style of Ornach-Nal Fault at the southernmost Hingol Basin (right).

**5.3.3. Base-level change related knickpoints**

The knickpoints in small tributaries are coextensive with the distance upstream of the terrace cliffs generated by the main valley incision in Cluster 2 (Figure 7). These knickpoints occur higher up in the bigger tributary catchments, especially in Cluster 1 (Figure 7). Considerably, the knickpoints have the same origin. In addition, the catchment size influences the rate of their upstream movement, as various field and experimental studies have shown (Parker, 1977; Schumm et al., 1987; Rosenbloom and Anderson, 1994; Bishop et al., 2005; Crosby and Whipple, 2006; Grimaud et al., 2016). The "stream power law," which connects stream power and river incision, where stream power is related to discharge, reflects this relationship (Howard, 1983; Howard et al., 1994; Seidl et al., 1994; Sklar and Dietrich, 2001; Loget et al., 2006; Berlin and Anderson, 2007; Royden and Perron, 2013). However, discharge statistics for tributary basins are sparse, so this idea should be verified, even if it is plausible.

The time required for the basin to readjust is another major element impacting the spatial placement of knickpoints within the river profile. By deducing upstream knickpoint migration, a tributary connecting the main channel downstream has more time to modify its profile than that connecting the main channel upstream. Longitudinal profiles of small tributary basins exhibit knickpoints nearer to their junction in the main channel than those of larger trunks (Figure 7).

In addition, the knickpoints were grouped into two clusters in the elevation vs. distance map (Figure 7). In Cluster 1, the knickpoints are less dense; some are even located at a similar elevation, inferring that these knickpoints with similar elevation could be formed by sea-level change as a uniform base-level lowering. The knickpoints in Cluster 2 are denser and are probably due to the Nai Rud Fault and its associated minor faults crossing the drainages and forming additional knickpoints (Figures 1, 5, and 7). Moreover, we infer that Cluster 1 locates the river course where the trunk river is across the ranges, and Cluster 2 locates where the trunk river flows alongside the ranges (Figure 5).

## 6. Conclusion

A complex drainage system that has undergone a number of changes over time is present in Pakistan's Eastern Makran. The index of active tectonics indicates moderate to low tectonic activity. Both the trunk streams and their tributaries have a variety of knickpoints. Different local variables influence the fluvial dynamics in the basin. We have classified the identified knickpoints into categories based on the individual or multiple mechanisms through which they were formed. Several knickpoints coincide with the major strikes that run through the basin, implying a link between drainage history and tectonic activities. Besides, the migratory knickpoints, comprising 59.81%, are indicated by the singular base-level fall. Moreover, 40.19% of knickpoints indicate enhanced

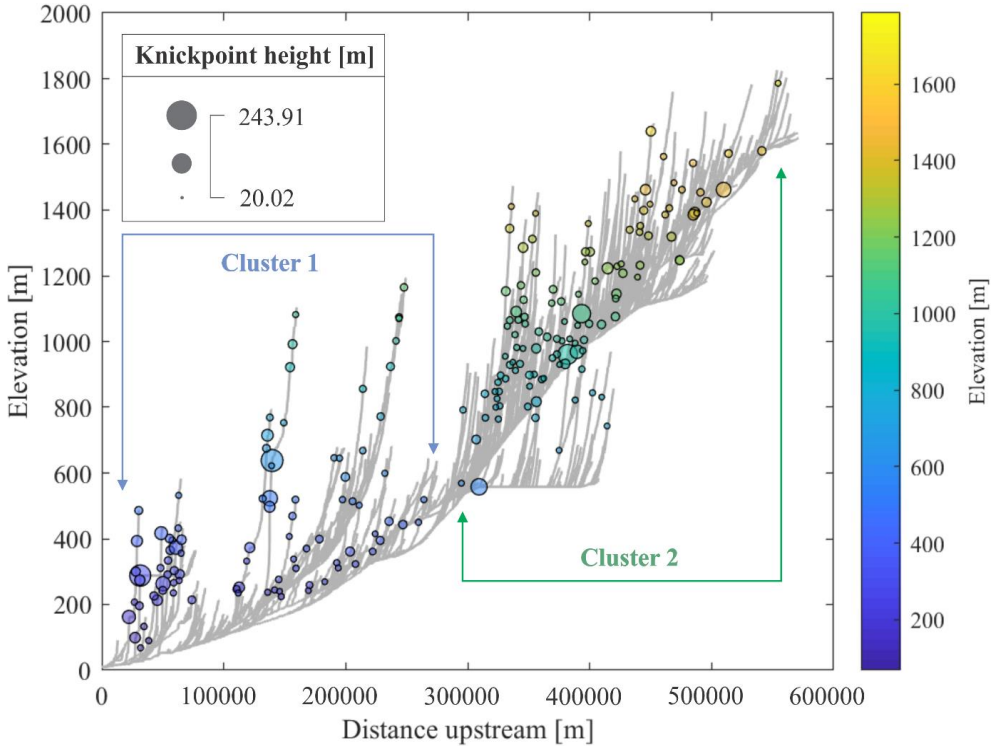


**Figure 7.** The plot showing the elevation vs. distance graph of the Hingol Drainage Basin divided into two clusters. Note that the knickpoint height (m) denotes the steps of the knickpoints in metres.

tectonic activities, for instance, fault initiation and/or increased fault slip. The results revealed that the northern edge of Nai Rud, between the Nai Rud and Ornach-Nal faults, and north of the Awaran Fault, experienced higher tectonic activity. Meanwhile, the subbasins with low tectonic activity are attributed to reduced erosive conditions and alluvial deposits. Lithology, particularly sedimentary covers, is regarded as one of the most vital variables controlling the streams' longitudinal profiles. The field evidence demonstrated that clastic rocks like massive and consolidated sandstone, mudstone, and conglomerate layers have a significant impact on the geomorphological indices. Moreover, the same tectonic stress is applied to the low-folded zone. Additionally, the similar temperature, climatic conditions, and rainfall led to the identical order, form, and size of the valleys in the southern parts.

**Acknowledgements**
We express our gratitude to the university fellows and experts for their invaluable assistance in enhancing the manuscript.

## References

Ascione A, Cinque A, Miccadei E, Villani F, Berti C (2008). The Plio-Quaternary uplift of the Apennine chain: new data from the analysis of topography and river valleys in Central Italy. Geomorphology, 102 (1): 105–118. https://doi.org/10.1016/j.geomorph.2007.07.022

Avouac JP, Ayoub F, Wei S, Ampuero JP, Meng L et al. (2014). The 2013, Mw 7.7 Balochistan earthquake, energetic strike-slip reactivation of a thrust fault. Earth and Planetary Science Letters, 391: 128–134. https://doi.org/10.1016/j.epsl.2014.01.036

Barnhart WD, Briggs RW, Reitman NG, Gold RD, Hayes GP (2015). Evidence for slip partitioning and bimodal slip behavior on a single fault: Surface slip characteristics of the 2013 Mw7.7 Balochistan, Pakistan earthquake. Earth and Planetary Science Letters, 420: 1–11. https://doi.org/10.1016/j.epsl.2015.03.027

Berlin MM, Anderson RS (2007). Modeling of knickpoint retreat on the Roan Plateau, western Colorado. Journal of Geophysical Research, 112 (F3): F03S06. https://doi.org/10.1029/2006JF000553

Bishop P, Hoey TB, Jansen JD, Artza IL (2005). Knickpoint recession rate and catchment area: the case of uplifted rivers in Eastern Scotland. Earth Surface Processes and Landforms, 30 (6): 767–778. https://doi.org/10.1002/esp.1191

Brookfield ME (1998). The evolution of the great river systems of southern Asia during the cenozoic India-Asia collision: rivers draining southwards. Geomorphology, 22 (3): 285–312.

Bull WB, McFadden LD (1977). Tectonic geomorphology north and south of the Garlock fault, California. In: Doehring, D.O. (Ed.), Geomorphology in Arid Regions. Proceedings of the Eighth Annual Geomorphology Symposium, 115–138.

Burbank DW, Anderson RS (2012). Tectonic Geomorphology (2nd ed.). Wiley-Blackwell.

Chen YC, Sung QC, Cheng KY (2003). Along-strike variations of morphotectonic features in the western foothills of Taiwan: tectonic implications based on stream gradient and hypsometric analysis. Geomorphology, 56: 109–137.

Clemens SC, Prell WL (2003). A 350,000 year summer-monsoon multi-proxy stack from the Owen Ridge, Northern Arabian Sea. Marine Geology, 201 (1–3): 35–51. https://doi.org/10.1016/S0025-3227(03)00207-X

Crosby BT, Whipple KX (2006). Knickpoint initiation and distribution within fluvial networks: 236 waterfalls in the Waipaoa River, North Island, New Zealand. Geomorphology, 82 (1–2): 16–38. https://doi.org/10.1016/j.geomorph.2005.08.023

Crupa WE, Khan SD, Huang J, Khan AS, Kasi A (2017). Active tectonic deformation of the western Indian plate boundary: A case study from the Chaman Fault System. Journal of Asian Earth Sciences, 147: 452–468. https://doi.org/10.1016/j.jseaes.2017.08.006

Delisle G, von Rad U, Andruleit H, von Daniels C, Tabrez A et al. (2002). Active mud volcanoes on- and offshore eastern Makran, Pakistan. International Journal of Earth Sciences, 91 (1): 93–110. https://doi.org/10.1007/s005310100203

Flint JJ (1974). Stream gradient as a function of order, magnitude, and discharge. Water Resources Research, 10 (5): 969–973. https://doi.org/10.1029/WR010i005p00969

Font M, Amorese D, Lagarde JL (2010). DEM and GIS analysis of the stream gradient index to evaluate effects of tectonics: The Normandy intraplate area (NW France). Geomorphology, 119 (3–4): 172–180. https://doi.org/10.1016/j.geomorph.2010.03.017

Fruehn J, White RS, Minshull TA (1997). Internal deformation and compaction of the Makran accretionary wedge. Terra Nova, 9 (3): 101–104. https://doi.org/10.1046/j.1365-3121.1997.d01-13.x

Giaconia F, Booth Rea G, Martínez Martínez JM, Azañón JM, Pérez Peña JV et al. (2012). Geomorphic evidence of active tectonics in the Sierra Alhamilla (eastern Betics, SE Spain). Geomorphology, 145–146: 90–106. https://doi.org/10.1016/j.geomorph.2011.12.043

Gilbert GK (1877). Geology of the Henry Mountains.

Goren L, Fox M, Willett SD (2014). Tectonics from fluvial topography using formal linear inversion: Theory and applications to the Inyo Mountains, California. Journal of Geophysical Research: Earth Surface, 119 (8): 1651–1681. https://doi.org/10.1002/2014JF003079

Grimaud JL, Paola C, Voller V (2016). Experimental migration of knickpoints: influence of style of base-level fall and bed lithology. Earth Surface Dynamics, 4 (1): 11–23. https://doi.org/10.5194/esurf-4-11-2016

Habibi A, Gharibreza M (2015). Estimation of the relative active tectonics in Shahriary basin (Central Iran) using geomorphic and seismicity indices. Natural Environment Change, 1 (1): 71–83.

Hack JT (1973). Stream-profile analysis and stream-gradient index. Journal of Research of the U.S. Geological Survey, 1 (4): 421–429.

Haghipour N, Burg JP (2014). Geomorphological analysis of the drainage system on the growing Makran accretionary wedge. Geomorphology, 209: 111–132. https://doi.org/10.1016/j.geomorph.2013.11.030

Haghipour N, Burg JP, Kober F, Zeilinger G, Ivy Ochs S et al. (2012). Rate of crustal shortening and non-Coulomb behaviour of an active accretionary wedge: The folded fluvial terraces in Makran (SE, Iran). Earth and Planetary Science Letters, 355–356: 187–198. https://doi.org/10.1016/j.epsl.2012.09.001

Hamdouni REl, Irigaray C, Fernandez T, Chac on J, Keller EA (2008). Assessment of relative active tectonics, southwest border of Sierra Nevada (Southern Spain). Geomorphology, 96: 150–173.

Hare PW, Gardner TW (1985). Geomorphic indicators of vertical neotectonism along converging plate margins, Nicoya Peninsula, Costa Rica. In: Morisawa, M., Hack, J.T. (Eds.), Tectonic Geomorphology, 75–104.

Harms JC, Cappel HN, Francis DC (1984). The Makran coast of Pakistan: its stratigraphy and hydrocarbon potential. In Marine Geology and Oceanography of Arabian Sea and Coastal Pakistan 3–26. Van Nostrand Reinhold.

Harms JC, Cappel HN, Francis DC (1982). Geology and Petroleum Potential of the Makran Coast, Pakistan. All Days. https://doi.org/10.2118/10423-MS

Harris I, Osborn TJ, Jones P, Lister D (2020). Version 4 of the CRU TS monthly high-resolution gridded multivariate climate dataset. Scientific Data, 7 (1): 109. https://doi.org/10.1038/s41597-020-0453-3

Howard ADKG (1983). Channel changes in badlands. Geological Society of America Bulletin, 94 (6): 739. https://doi.org/10.1130/0016-7606(1983)94<739:CCIB>2.0.CO;2

Howard AD, Dietrich WE, Seidl MA (1994). Modeling fluvial erosion on regional to continental scales. Journal of Geophysical Research: Solid Earth, 99 (B7): 13971–13986. https://doi.org/10.1029/94JB00744

Huang J, Khan S, Khan AS (2016). Slip rates of Chaman Fault System, Pakistan. https://doi.org/10.1130/abs/2016AM-281010

Hunting Survey Corporation (1960). Reconnaissance geology of part of West Pakistan : a Colombo Plan Cooperative Project. Government of Canada for the Government of Pakistan.

Huyghe P, Foata M, Deville E, Mascle G, Group CW (2004). Channel profiles through the active thrust front of the southern Barbados prism. Geology, 32 (5): 429–432. https://doi.org/10.1130/G20000.1

Jaiswara NK, Kotluri SK, Pandey AK, Pandey P (2019). Transient basin as indicator of tectonic expressions in bedrock landscape: Approach based on MATLAB geomorphic tool (Transient-profiler). Geomorphology, 346: 106853. https://doi.org/10.1016/j.geomorph.2019.106853

Joshi LM, Kotlia BS (2018). Tectonic footprints and landscape evaluation along Kulur River valley, Kumaun Lesser Himalaya, India. Journal of Asian Earth Sciences, 162: 121–136. https://doi.org/10.1016/j.jseaes.2018.04.023

Kassi AM, Grigsby JD, Khan AS, Kasi AK (2015). Sandstone petrology and geochemistry of the Oligocene–Early Miocene Panjgur Formation, Makran accretionary wedge, southwest Pakistan: Implications for provenance, weathering and tectonic setting. Journal of Asian Earth Sciences, 105: 192–207. https://doi.org/10.1016/j.jseaes.2015.03.021

Kehl M (2009). Quaternary climate change in Iran – the state of knowledge. ERDKUNDE, 63 (1): 1–17. https://doi.org/10.3112/erdkunde.2009.01.01

Keller EA, Pinter N (2002). Active Tectonics: Earthquakes, Uplift, and Landscape. Prentice Hall, Upper Saddle River, New Jersey.

Khan W, Dost C, Murad F, Muhammad A, Ahmed F (2022). Neotectonic Activity in Quetta-Ziarat Region, Northwest Quetta City, Pakistan. International Journal of Economic and Environmental Geology, 13 (4): 24–28. https://doi.org/10.46660/ijeeg.v13i4.49

Khan W, Zhang K, Liang H, Yu P (2023a). Provenance for the Makran Flysch Basin in Pakistan: implications for interaction between the Indian, Eurasian, and Arabian Plates. Journal of Asian Earth Sciences, 105626. https://doi.org/10.1016/j.jseaes.2023.105626

Khan W, Zhang K, Liang H, Yu P (2023b). Geochemical Assessment of River Sediments at the Outlets of Eastern Makran, Pakistan; Implications for Source Area Weathering and Provenance. Minerals, 13 (3): 348. https://doi.org/10.3390/min13030348

Kirby E, Whipple K (2001). Quantifying differential rock-uplift rates via stream profile analysis. Geology, 29 (5): 415. https://doi.org/10.1130/0091-7613(2001)029<0415:QDRURV>2.0.CO;2

Klinkenberg B (1992). Fractals and morphometric measures: is there a relationship? Geomorphology, 5 (1–2): 5–20. https://doi.org/10.1016/0169-555X(92)90055-S

Kobor JS, Roering JJ (2004). Systematic variation of bedrock channel gradients in the central Oregon Coast Range: implications for rock uplift and shallow landsliding. Geomorphology, 62 (3–4): 239–256. https://doi.org/10.1016/j.geomorph.2004.02.013

Liu Z, Han L, Boulton SJ, Wu T, Guo J (2020). Quantifying the transient landscape response to active faulting using fluvial geomorphic analysis in the Qianhe Graben on the southwest margin of Ordos, China. Geomorphology, 351: 106974. https://doi.org/10.1016/j.geomorph.2019.106974

Loget N, Davy P, van den Driessche J (2006). Mesoscale fluvial erosion parameters deduced from modeling the Mediterranean sea level drop during the Messinian (late Miocene). Journal of Geophysical Research: Earth Surface, 111 (F3): n/a-n/a. https://doi.org/10.1029/2005JF000387

Lykoudi E, Angelaki M (2004). The contribution of the morphometric parameters of a hydrographic network to the investigation of the neotectonic activity: an application to the upper Acheloos River. Proceedings of the 10th International Congress, Thessaloniki, 1084–1092.

Mackin JH (1948). Concept of the graded river. Bulletin of the Geological Society of America, 59: 463–512.

Masson F, Chéry J, Hatzfeld D, Martinod J, Vernant P et al. (2004). Seismic versus aseismic deformation in Iran inferred from earthquakes and geodetic data. Geophysical Journal International, 160 (1): 217–226. https://doi.org/10.1111/j.1365-246X.2004.02465.x

Mayer L (1990). Introduction to Quantitative Geomorphology. Prentice Hall, Englewood, Cliffs, NJ.

Mouchot N, Loncke L, Mahieux G, Bourget J, Lallemant S et al. (2010). Recent sedimentary processes along the Makran trench (Makran active margin, off Pakistan). Marine Geology, 271 (1–2): 17–31. https://doi.org/10.1016/j.margeo.2010.01.006

Nourbakhsh A (2014). Quantitative Analysis of Geomorphic Responses to Active Tectonic Process in the Zagros Orogenic Belt, Iran [Ph.D]. Shiraz University.

Pánek T (2004). The use of morphometric parameters in tectonic geomorphology (on the example of the Western Beskydy Mts). Acta Universitatis Carolinae, Geographica, 1: 111–126.

Parker RS (1977). Experimental study of basin evolution and its hydrologic implications [PhD]. Colorado State University, Fort Collins.

Piacentini D, Troiani F, Servizi T, Nesci O, Veneri F (2020). SLiX: A GIS Toolbox to Support Along-Stream Knickzones Detection through the Computation and Mapping of the Stream Length-Gradient (SL) Index. ISPRS International Journal of Geo-Information, 9 (2): 69. https://doi.org/10.3390/ijgi9020069

Pike RJ, Wilson SE (1971). Elevation-relief ratio, hypsometric integral, and geomorphic area altitude analysis. GSA Bulletin, 82 (4): 1079–1084.

Rosenbloom NA, Anderson RS (1994). Hillslope and channel evolution in a marine terraced landscape, Santa Cruz, California. Journal of Geophysical Research: Solid Earth, 99 (B7): 14013–14029. https://doi.org/10.1029/94JB00048

Royden L, Perron JT (2013). Solutions of the stream power equation and application to the evolution of river longitudinal profiles. Journal of Geophysical Research: Earth Surface, 118 (2): 497–518. https://doi.org/10.1002/jgrf.20031

Ruleman CA (2005). Annotated Bibliography for Quaternary Faulting and Geomorphic Tectono-morphic Development of Afghanistan e Progress Report for Afghan Geologic Hazards Activities.

Schlüter HU, Prexl A, Gaedicke Ch, Roeser H, Reichert Ch et al. (2002). The Makran accretionary wedge: sediment thicknesses and ages and the origin of mud volcanoes. Marine Geology, 185 (3–4): 219–232. https://doi.org/10.1016/S0025-3227(02)00192-5

Schumm SA, Mosley MP, Weaver WE (1987). Experimental Fluvial Geomorphology. John Wiley and Sons.

Schwanghart W, Scherler D (2014). Short Communication: TopoToolbox 2 – MATLAB-based software for topographic analysis and modeling in Earth surface sciences. Earth Surface Dynamics, 2 (1): 1–7. https://doi.org/10.5194/esurf-2-1-2014

Schwanghart W, Molkenthin C, Scherler D (2021). A systematic approach and software for the analysis of point patterns on river networks. Earth Surface Processes and Landforms, 46 (9): 1847-1862. https://doi.org/10.1002/esp.5127

Schwanghart W (2021). Examples of PPS (Point pattern on stream networks) for TopoToolbox. In Earth surface processes and landforms (1.0). Zenodo. https://doi.org/10.5281/zenodo.4658411

Seidl MA, Dietrich WE, Kirchner JW (1994). Longitudinal Profile Development into Bedrock: An Analysis of Hawaiian Channels. The Journal of Geology, 102 (4): 457–474.

Shah ST (2019). Fault based probabilistic seismic hazard assessment at different tectonic regimes and data sampling conditions: emphasis on sensitivity of seismic source characterization PhD, Middle East Technical University, Ankara, Türkiye.

Shah ST, Özacar AA, Gülerce Z (2021). Fault-based probabilistic seismic hazard assessment of the eastern Makran subduction and the Chaman transform fault, Pakistan: Emphasis on the source characterization of megathrust. Journal of Asian Earth Sciences, 205: 104604. https://doi.org/10.1016/j.jseaes.2020.104604

Silva PG, Goy JL, Zazo C, Bardajî T (2003). Fault-generated mountain fronts in southeast Spain: geomorphologic assessment of tectonic and seismic activity. Geomorphology, 50 (1–3): 203–225. https://doi.org/10.1016/S0169-555X(02)00215-5

Sklar LS, Dietrich WE (2001). Sediment and rock strength controls on river incision into bedrock. Geology, 29 (12): 1087. https://doi.org/10.1130/0091-7613(2001)029<1087:SARSCO>2.0.CO;2

Smith G, McNeill L, Henstock TJ, Bull J (2012). The structure and fault activity of the Makran accretionary prism. Journal of Geophysical Research: Solid Earth, 117 (B7): n/a-n/a. https://doi.org/10.1029/2012JB009312

Snyder NP, Whipple KX, Tucker GE, Merritts DJ (2003). Importance of a stochastic distribution of floods and erosion thresholds in the bedrock river incision problem. Journal of Geophysical Research: Solid Earth, 108 (B2). https://doi.org/10.1029/2001JB001655

Strahler A (1952). Hypsometric (area-altitude) analysis of erosional topography. Geological Society of America Bulletin, 63 (11): 1117–1142.

Summerfield MA (1999). Geomorphology and global tectonics. John Wiley & Sons, Ltd. Press.

Székely B (2001). On the surface of the Eastern Alps-A DEM study. University Tübingen Press.

Topal S, Keller E, Bufe A, Koçyiğit A (2016). Tectonic geomorphology of a large normal fault: Akşehir fault, SW Turkey. Geomorphology, 259: 55–69. https://doi.org/10.1016/j.geomorph.2016.01.014

Tucker GE, Whipple KX (2002). Topographic outcomes predicted by stream erosion models: Sensitivity analysis and intermodel comparison. Journal of Geophysical Research: Solid Earth, 107 (B9): ETG 1-1-ETG 1-16. https://doi.org/10.1029/2001JB000162

Whipple KX, DiBiase RA, Crosby BT (2013). Bedrock Rivers. In Treatise on Geomorphology 550–573. Elsevier. https://doi.org/10.1016/B978-0-12-374739-6.00254-2

Wobus C, Whipple KX, Kirby E, Snyder N, Johnson J et al. (2006). Tectonics from topography: Procedures, promise, and pitfalls. In Tectonics, Climate, and Landscape Evolution 55–74. Geological Society of America. https://doi.org/10.1130/2006.2398(04)

Zhang J, Shan X, Huang X (2011). Seismotectonics in the Pamir: An oblique transpressional shear and south-directed deep-subduction model. Geoscience Frontiers, 2 (1): 1–15. https://doi.org/10.1016/j.gsf.2010.11.002

Zhou Y, Walker RT, Elliott JR, Parsons B (2016). Mapping 3D fault geometry in earthquakes using high-resolution topography: Examples from the 2010 El Mayor-Cucapah (Mexico) and 2013 Balochistan (Pakistan) earthquakes. Geophysical Research Letters, 43 (7): 3134–3142. https://doi.org/10.1002/2016GL067899

Zygouri V, Koukouvelas IK, Kokkalas S, Xypolias P, Papadopoulos GA (2015). The Nisi Fault as a key structure for understanding the active deformation of the NW Peloponnese, Greece. Geomorphology, 237: 142–156. https://doi.org/10.1016/j.geomorph.2013.09.001

**Appendix.** The generated knickpoints of the Hingol Drainage Basin in Pakistan. Here, basin no. refers to the subbasins in which the knickpoints fall, type 1 refers to fixed/vertical-step knickpoints and 2 refers to migratory/slope-break knickpoints.

| ID | KP height (m) | Elevation | Distance upstream | Area (km$^2$) | Subbasin no. | Type | Remarks | Range |
|---|---|---|---|---|---|---|---|---|
| 1 | 243.91 | 638 | 139604.5 | 67.42 | 29 | 1 | On the same lithology (Tnh) | 5 |
| 2 | 227.18 | 288 | 31518.41 | 580.85 | 40 | 1 | On the same lithology (Tnh) | 5 |
| 3 | 45.64 | 922 | 154333.2 | 21.55 | 29 | 1 | On the same lithology (Tnh) | 4 |
| 4 | 197.36 | 961 | 381960.5 | 4669.5 | 15 | 2 | On the same lithology (TK) close to a fault | 5 |
| 5 | 44.19 | 992 | 156387.5 | 12.19 | 29 | 1 | On the same lithology (Tnh) | 2 |
| 6 | 39.88 | 365 | 56040.02 | 33.5 | 40 | 1 | On the same lithology (Tnh) | 2 |
| 7 | 24.17 | 753 | 149181.5 | 33.61 | 29 | 1 | On the same lithology (Tnh) | 1 |
| 8 | 168.23 | 1085 | 393379.9 | 602.67 | 10 | 2 | Lithological differences but close to a major fault | 5 |
| 9 | 62.32 | 1392 | 486086.2 | 93.13 | 9 | 1 | Lithological differences | 3 |
| 10 | 22.16 | 1082 | 158944.2 | 10.48 | 29 | 1 | On the same lithology (Tnh) | 1 |
| 11 | 25.19 | 395 | 57802.81 | 9.32 | 40 | 1 | On the same lithology (Tnh) | 1 |
| 12 | 22.11 | 532 | 62983.6 | 12.16 | 40 | 1 | On the same lithology (Tnh) | 1 |
| 13 | 136.05 | 558 | 309292.2 | 2752.54 | 21 | 1 | Lithological differences but close to a major fault | 5 |
| 14 | 62.05 | 1386 | 485004.7 | 445.76 | 9 | 1 | Lithological differences | 3 |
| 15 | 64.14 | 1223 | 414715.7 | 357.8 | 10 | 2 | Lithological differences but close to a major fault | 3 |
| 16 | 52.43 | 817 | 356306.2 | 28.38 | 27 | 2 | On the same lithology (TK) close to a fault | 3 |
| 17 | 49.84 | 1145 | 421945.3 | 75.4 | 14 | 2 | On the same lithology (TK) close to a fault | 3 |
| 18 | 122.22 | 523 | 137758.2 | 70.29 | 29 | 1 | On the same lithology (Tnh) | 4 |
| 19 | 24.91 | 1184 | 404518.3 | 55.36 | 10 | 2 | Lithological differences but close to a major fault | 1 |
| 20 | 22.3 | 1434 | 437034.7 | 13.26 | 10 | 2 | Lithological differences but close to a major fault | 1 |
| 21 | 47.69 | 979 | 356145.4 | 23.53 | 27 | 2 | On the same lithology (TK) close to a fault | 3 |
| 22 | 40.22 | 1076 | 421052.1 | 286.31 | 13 | 1 | Lithological differences | 2 |
| 23 | 112.69 | 1462 | 509798.5 | 1095.61 | 1 | 2 | On the same lithology (Tpgd) close to a fault | 4 |
| 24 | 21.36 | 622 | 139194.9 | 69.04 | 29 | 1 | On the same lithology (Tnh) | 1 |
| 25 | 34.18 | 1014 | 365096 | 14.93 | 27 | 2 | On the same lithology (TK) close to a fault | 2 |
| 26 | 40.08 | 1052 | 409680.4 | 3733.44 | 14 | 2 | On the same lithology (TK) close to a fault | 2 |

| | | | | | | | | |
|---|---|---|---|---|---|---|---|---|
| 27 | 107.49 | 263 | 50233.89 | 33.67 | 39 | 1 | On the same lithology (Tnh) | 4 |
| 28 | 39.72 | 1580 | 541134.1 | 501.04 | 1 | 2 | On the same lithology (Tnh | 3 |
| 29 | 31.54 | 768 | 355557.4 | 59.64 | 27 | 2 | On the same lithology (TK) close to a fault | 2 |
| 30 | 26.6 | 1462 | 475609.3 | 11.44 | 9 | 2 | On the same lithology (TK) close to a faul | 1 |
| 31 | 95.88 | 969 | 389556.2 | 4051.27 | 6 | 2 | On the same lithology (TK) close to a fault | 4 |
| 32 | 23.51 | 1563 | 460563.8 | 36.44 | 12 | 2 | On the same lithology (TK) close to a fault | 1 |
| 33 | 39.67 | 401 | 55478.36 | 11.19 | 39 | 1 | On the same lithology (Tnh) | 2 |
| 34 | 20.79 | 1786 | 554464.5 | 21.08 | 1 | 2 | On the same lithology (JS) close to a fault | 1 |
| 35 | 31.2 | 1054 | 399518.5 | 17.46 | 28 | 2 | On the same lithology (TK) close to a fault | 2 |
| 36 | 93.61 | 373 | 60738.74 | 20.75 | 39 | 1 | On the same lithology (Tnh) | 4 |
| 37 | 28.12 | 885 | 360747.5 | 43.23 | 27 | 2 | On the same lithology (TK) close to a fault | 1 |
| 38 | 20.65 | 1418 | 449447.9 | 20.53 | 12 | 2 | On the same lithology (TK) close to a fault | 1 |
| 39 | 49.81 | 1424 | 495793.3 | 229.17 | 1 | 2 | On the same lithology (Tpgd) close to a fault | 3 |
| 40 | 31.09 | 1005 | 395333 | 13.23 | 28 | 2 | On the same lithology (TK) close to a fault | 2 |
| 41 | 90.53 | 162 | 22264.7 | 31.31 | 41 | 1 | On the same lithology (Tnh) | 4 |
| 42 | 20.52 | 1049 | 390148.6 | 17.07 | 15 | 2 | On the same lithology (TK) close to a fault | 1 |
| 43 | 26.05 | 432 | 62716.19 | 11 | 39 | 1 | On the same lithology (Tnh) | 1 |
| 44 | 43.82 | 1319 | 467042.3 | 13.92 | 5 | 2 | On the same lithology (Ton) close to a fault | 2 |
| 45 | 25.07 | 916 | 393570.3 | 52.16 | 28 | 2 | On the same lithology (TK) close to a fault | 1 |
| 46 | 86.61 | 417 | 48691.23 | 13.34 | 39 | 1 | On the same lithology (Tnh) | 4 |
| 47 | 65.28 | 393 | 28801.47 | 11.12 | 41 | 1 | On the same lithology (Tnh | 3 |
| 48 | 43.05 | 1248 | 473612.1 | 1695.58 | 1,3,4 | 1 | Lithological differences | 2 |
| 49 | 24.44 | 972 | 394344.3 | 14.5 | 28 | 2 | On the same lithology (TK) close to a fault | 1 |
| 50 | 71.89 | 715 | 135818.1 | 21.48 | 29 | 1 | On the same lithology (Tnh) | 4 |
| 51 | 36 | 486 | 30292.51 | 9.53 | 41 | 1 | On the same lithology (Tnh) | 2 |
| 52 | 45.2 | 300 | 27889.6 | 11.86 | 41 | 1 | On the same lithology (Tnh) | 2 |
| 53 | 42.62 | 1247 | 473874.5 | 413.22 | 4 | 1 | Lithological differences | 2 |
| 54 | 31.63 | 1454 | 490779.4 | 46.37 | 1 | 2 | On the same lithology (Tnh) close to a fault | 2 |
| 55 | 24.1 | 900 | 354468.8 | 27.92 | 27 | 2 | On the same lithology (TK) close to a fault | 1 |
| 56 | 62.45 | 497 | 137627 | 70.3 | 29 | 1 | On the same lithology (Tnh) | 3 |

| | | | | | | | | |
|---|---|---|---|---|---|---|---|---|
| 57 | 24.28 | 207 | 26769.67 | 12.55 | 41 | 1 | On the same lithology (Tnh) | 1 |
| 58 | 27.43 | 769 | 137818 | 10.68 | 29 | 1 | On the same lithology (Tnh) | 1 |
| 59 | 34.17 | 1572 | 513916.4 | 60.17 | 4 | 2 | On the same lithology (Tnh) close to a fault | 2 |
| 60 | 40.13 | 1208 | 427195.3 | 16.17 | 6 | 2 | On the same lithology (Tnh) close to a fault | 2 |
| 61 | 22.8 | 844 | 402288.7 | 22.35 | 28 | 2 | On the same lithology (TK) close to a fault | 1 |
| 62 | 60.57 | 1091 | 339764.8 | 18.23 | 11 | 2 | On the same lithology (TK) close to a fault | 3 |
| 63 | 37.24 | 1399 | 444295.1 | 21.68 | 6 | 2 | Lithological differences (TB) close to a fault | 2 |
| 64 | 22.13 | 822 | 388095.2 | 45.54 | 28 | 2 | On the same lithology (TK) close to a fault | 1 |
| 65 | 60.41 | 252 | 112671.7 | 38.86 | 36 | 1 | Lithological differences | 3 |
| 66 | 34.96 | 1232 | 441268 | 58.42 | 6 | 2 | On the same lithology (Ton) close to a fault | 2 |
| 67 | 21.31 | 669 | 374934.4 | 32.96 | 28 | 2 | On the same lithology (TK) close to a fault | 1 |
| 68 | 59.62 | 99 | 27301.1 | 595.62 | 40 | 1 | On the same lithology (Tnh) | 3 |
| 69 | 29.35 | 1543 | 484689.5 | 11.83 | 5 | 2 | On the same lithology (JS) close to a fault | 1 |
| 70 | 20.66 | 743 | 414272.5 | 21.14 | 28 | 2 | On the same lithology (TK) close to a fault | 1 |
| 71 | 58.68 | 213 | 45462.64 | 20.85 | 39 | 1 | On the same lithology (Tnh) | 3 |
| 72 | 57.33 | 274 | 31163.21 | 581.01 | 40 | 1 | On the same lithology (Tnh | 3 |
| 73 | 26.8 | 1131 | 421349.1 | 77.56 | 6 | 2 | On the same lithology (Tnh) close to a fault | 1 |
| 74 | 20.16 | 831 | 409915.8 | 28.6 | 28 | 2 | On the same lithology (TK) close to a fault | 1 |
| 75 | 58.38 | 1462 | 445765.9 | 32.15 | 8 | 2 | On the same lithology (TK) close to a fault | 3 |
| 76 | 28.5 | 311 | 48150.48 | 13.65 | 39 | 1 | On the same lithology (Tnh) | 1 |
| 77 | 35.19 | 196 | 30808.02 | 583.92 | 40 | 1 | On the same lithology (Tnh | 2 |
| 78 | 26.04 | 1386 | 461922.5 | 36.21 | 3 | 2 | On the same lithology (Tnh) close to a fault | 1 |
| 79 | 54.55 | 373 | 121317.2 | 99.16 | 29 | 1 | On the same lithology (Tnh) | 3 |
| 80 | 20.22 | 1196 | 439236.2 | 67.47 | 6 | 2 | On the same lithology (Tnh) close to a faul | 1 |
| 81 | 50.84 | 1286 | 345387 | 15.69 | 11 | 1 | Lithological differences | 3 |
| 82 | 34.29 | 675 | 134976.5 | 22.97 | 29 | 1 | On the same lithology (Tnh) | 2 |
| 83 | 50.35 | 1640 | 450152.8 | 13.74 | 8 | 2 | On the same lithology (TK) close to a faul | 3 |
| 84 | 29.02 | 522 | 131917.5 | 40.02 | 29 | 1 | On the same lithology (Tnh) | 1 |
| 85 | 49.31 | 932 | 379928.7 | 2617.2 | 8 | 2 | Lithological differences but close to a fault and earthquake area | 3 |
| 86 | 48.85 | 397 | 65381.51 | 9.73 | 39 | 1 | On the same lithology (Tnh) | 3 |

| | | | | | | | | |
|---|---|---|---|---|---|---|---|---|
| 87 | 42.06 | 1273 | 400302.1 | 10.61 | 8 | 2 | On the same lithology (TK) close to a fault and earthquake | 2 |
| 88 | 21.14 | 1144 | 390788.7 | 9.43 | 8 | 2 | On the same lithology (TK) close to a fault and earthquake | 1 |
| 89 | 48.07 | 292 | 63890.47 | 30.19 | 39 | 1 | On the same lithology (Tnh | 3 |
| 90 | 36.56 | 1273 | 396589.8 | 31.65 | 8 | 2 | On the same lithology (TK) close to a fault and earthquake | 2 |
| 91 | 45.09 | 361 | 203525.6 | 26.69 | 26 | 2 | On the same lithology (TK) close to a fault | 2 |
| 92 | 23.17 | 356 | 65026.32 | 9.98 | 39 | 1 | On the same lithology (Tnh | 1 |
| 93 | 34.4 | 1322 | 448143.5 | 11.95 | 8 | 2 | On the same lithology (TK) close to a fault | 2 |
| 94 | 21.58 | 1359 | 398884.1 | 28.28 | 8 | 2 | On the same lithology (TK) close to a fault and earthquake | 1 |
| 95 | 44.1 | 1153 | 331249.5 | 20.42 | 11 | 2 | On the same lithology (TK) close to a fault | 2 |
| 96 | 22.75 | 502 | 210978.1 | 9.37 | 26 | 2 | On the same lithology (TK) close to a fault | 1 |
| 97 | 29.27 | 1340 | 432809.2 | 15.95 | 8 | 2 | Lithological difference but close to a fault and earthquake | 1 |
| 98 | 41.85 | 702 | 306984.8 | 1276.7 | 17 | 2 | On the same lithology (TK) close to a fault | 2 |
| 99 | 27.34 | 1406 | 465214.3 | 27.81 | 8 | 2 | On the same lithology (TK) close to a fault | 1 |
| 100 | 39.39 | 1344 | 334439.6 | 14.25 | 11 | 2 | On the same lithology (TK) close to a fault | 2 |
| 101 | 40.88 | 588 | 199664.7 | 10.51 | 30 | 1 | On the same lithology (Tnh) | 2 |
| 102 | 29.52 | 929 | 334659.8 | 45.61 | 17 | 2 | On the same lithology (TK) close to a fault | 1 |
| 103 | 26.14 | 1352 | 441500.8 | 31.26 | 8 | 2 | On the same lithology (TK) close to a fault | 1 |
| 104 | 21.33 | 1411 | 335799.5 | 11.47 | 11 | 2 | On the same lithology (TK) close to a fault | 1 |
| 105 | 21.43 | 1483 | 469098.9 | 18.82 | 8 | 2 | On the same lithology (TK) close to a fault | 1 |
| 106 | 39.98 | 443 | 246866.4 | 605.65 | 22 | 2 | On the same lithology (TK) | 2 |
| 107 | 26.01 | 887 | 331015 | 68.63 | 17 | 2 | On the same lithology (TK) close to a fault | 1 |
| 108 | 25.82 | 1333 | 440921.6 | 55.23 | 8 | 2 | On the same lithology (TK) close to a fault | 1 |
| 109 | 38.23 | 453 | 235520 | 26.92 | 26 | 2 | On the same lithology (TK) | 2 |
| 110 | 25.45 | 848 | 325754.7 | 43.33 | 17 | 2 | On the same lithology (TK) close to a fault | 1 |
| 111 | 24.06 | 1229 | 422390.6 | 21.79 | 8 | 2 | Lithological differences but close to a fault and earthquake area | 1 |
| 112 | 37.81 | 226 | 42819.83 | 10.6 | 42 | 2 | On the same lithology (Tnh) but close to a fault | 2 |
| 113 | 24.25 | 1117 | 368891.3 | 16.48 | 17 | 2 | On the same lithology (TK) | 1 |
| 114 | 22.71 | 1236 | 425840.4 | 9.77 | 8 | 2 | On the same lithology (TK) close to a fault | 1 |
| 115 | 37.23 | 395 | 228227.8 | 15179.96 | 26 | 2 | On the same lithology (TK) close to a fault | 2 |
| 116 | 23.77 | 804 | 326263.6 | 571.39 | 17 | 2 | On the same lithology (TK) | 1 |

| | | | | | | | | |
|---|---|---|---|---|---|---|---|---|
| 117 | 22.25 | 1391 | 487901.7 | 158.54 | 7 | 1 | Lithological differences | 1 |
| 118 | 36.65 | 303 | 59433.25 | 21.69 | 39 | 1 | On the same lithology (Tnh) | 2 |
| 119 | 22.21 | 912 | 339139.5 | 12.66 | 17 | 2 | On the same lithology (TK) close to a fault | 1 |
| 120 | 30.96 | 1122 | 376610 | 19.48 | 8 | 2 | On the same lithology (TK) close to a fault and earthquake | 2 |
| 121 | 23.54 | 1047 | 332435.8 | 22.56 | 17 | 2 | On the same lithology (TK) | 1 |
| 122 | 20.46 | 1242 | 396087.5 | 33.49 | 8 | 2 | On the same lithology (TK) | 1 |
| 123 | 35.7 | 924 | 236725.6 | 88.18 | 19 | 2 | On the same lithology (TK) | 2 |
| 124 | 30.27 | 1075 | 346592 | 9.21 | 16 | 2 | On the same lithology (TK) close to a fault | 2 |
| 125 | 21.46 | 848 | 322394.9 | 88.42 | 17 | 2 | On the same lithology (TK) | 1 |
| 126 | 35.2 | 243 | 49955.56 | 33.8 | 39 | 1 | On the same lithology (Tnh) | 2 |
| 127 | 28.77 | 961 | 373103.1 | 15.86 | 15 | 2 | On the same lithology (TK) close to a fault | 1 |
| 128 | 20.37 | 800 | 323066.8 | 80.22 | 17 | 2 | On the same lithology (TK) close to a fault | 1 |
| 129 | 31.62 | 1165 | 247771.2 | 10.56 | 19 | 2 | On the same lithology (TK) close to a fault | 2 |
| 130 | 35.19 | 214 | 73865.02 | 23.18 | 42 | 1 | On the same lithology (Tnh) | 2 |
| 131 | 28.26 | 1065 | 334484.7 | 19.51 | 21 | 2 | On the same lithology (TK) | 1 |
| 132 | 20.15 | 937 | 336915.6 | 54.66 | 17 | 2 | On the same lithology (TK) close to a thrust | 1 |
| 133 | 28.83 | 1074 | 243777.9 | 9.33 | 19 | 2 | On the same lithology (TK) | 1 |
| 134 | 33.74 | 1159 | 369973.9 | 13.07 | 11 | 1 | Lithological differences | 2 |
| 135 | 27.49 | 897 | 326942.1 | 10.24 | 16 | 2 | On the same lithology (TK) close to a fault | 1 |
| 136 | 25.75 | 1002 | 241205.4 | 61.16 | 19 | 2 | On the same lithology (TK) close to a fault | 1 |
| 137 | 33.23 | 1030 | 358371.6 | 16.85 | 11 | 2 | On the same lithology (TK) close to a fault | 2 |
| 138 | 24.12 | 876 | 324914.2 | 11.23 | 21 | 2 | On the same lithology (TK) | 1 |
| 139 | 24 | 1070 | 243669.2 | 21.42 | 19 | 2 | On the same lithology (TK) close to a fault | 1 |
| 140 | 33.2 | 898 | 350599.6 | 71.55 | 11 | 2 | On the same lithology (TK) close to a fault | 2 |
| 141 | 22.93 | 982 | 340182.6 | 8.98 | 16 | 2 | On the same lithology (TK) close to a fault | 1 |
| 142 | 33.19 | 399 | 178389.8 | 28.77 | 19 | 1 | Lithological differences | 2 |
| 143 | 21.62 | 1002 | 377381.4 | 48.03 | 15 | 2 | On the same lithology (TK) close to a fault | 1 |
| 144 | 32.6 | 1312 | 353009.1 | 19.56 | 11 | 2 | On the same lithology (TK) close to a fault | 2 |
| 145 | 21.6 | 826 | 324111 | 95.25 | 21 | 2 | On the same lithology (TK) | 1 |
| 146 | 31.71 | 334 | 54374.34 | 9.58 | 39 | 1 | On the same lithology (Tnh) | 2 |

| | | | | | | | | |
|---|---|---|---|---|---|---|---|---|
| 147 | 20.02 | 955 | 330776.3 | 23.3 | 21 | 2 | On the same lithology (TK) | 1 |
| 148 | 20.63 | 979 | 345286.5 | 11.04 | 16 | 2 | On the same lithology (TK) close to a fault | 1 |
| 149 | 20.39 | 1390 | 355658.5 | 15.22 | 11 | 1 | Lithological differences | 1 |
| 150 | 31.64 | 841 | 314067.3 | 16.95 | 11 | 2 | On the same lithology (TK) | 2 |
| 151 | 20.13 | 930 | 375327.1 | 4693.75 | 15 | 2 | On the same lithology (TK) close to a fault | 1 |
| 152 | 31.56 | 772 | 228607.8 | 126.08 | 19 | 2 | On the same lithology (TK) close to a fault | 2 |
| 153 | 31.46 | 469 | 156383.7 | 15.27 | 30 | 1 | On the same lithology (Tnh) | 2 |
| 154 | 31.44 | 291 | 53926.37 | 10.13 | 39 | 1 | On the same lithology (Tnh) | 2 |
| 155 | 27.43 | 519 | 158770.7 | 11.92 | 30 | 1 | On the same lithology (Tnh) | 1 |
| 156 | 31.26 | 1210 | 355866.6 | 14.99 | 11 | 1 | Lithological differences | 2 |
| 157 | 30.74 | 1127 | 345825.7 | 59.71 | 11 | 1 | Lithological differences | 2 |
| 158 | 30.67 | 1171 | 343595.1 | 19.07 | 11 | 1 | Lithological differences | 2 |
| 159 | 30 | 247 | 110441.2 | 9.03 | 36 | 1 | Lithological differences | 2 |
| 160 | 28.94 | 932 | 342837 | 50.9 | 11 | 2 | On the same lithology (TK) | 1 |
| 161 | 28.61 | 856 | 214028.9 | 14.7 | 25 | 2 | On the same lithology (TK) close to a fault | 1 |
| 162 | 25.79 | 1054 | 347047.7 | 15.3 | 11 | 2 | On the same lithology (TK) | 1 |
| 163 | 28.02 | 1008 | 373141.5 | 31.42 | 11 | 2 | On the same lithology (TK) | 1 |
| 164 | 27.92 | 514 | 205638.2 | 41.25 | 30 | 1 | On the same lithology (Tnh) | 1 |
| 165 | 27.81 | 259 | 170325.2 | 36.06 | 36 | 1 | Lithological differences | 1 |
| 166 | 26.25 | 668 | 213925.7 | 16.9 | 30 | 1 | On the same lithology (Tnh) | 1 |
| 167 | 27.41 | 1066 | 341509 | 26.91 | 11 | 2 | On the same lithology (TK | 1 |
| 168 | 27.1 | 802 | 349287.6 | 5288.24 | 11 | 1 | Lithological differences | 1 |
| 169 | 26.73 | 361 | 222069.9 | 533.22 | 36 | 2 | On the same lithology (TK) close to a fault | 1 |
| 170 | 26.45 | 950 | 369487.5 | 38.06 | 11 | 2 | On the same lithology (TK) | 1 |
| 171 | 26.57 | 370 | 167852 | 324.16 | 32 | 2 | On the same lithology (TK) | 1 |
| 172 | 21.52 | 995 | 388042.7 | 625.67 | 10,11 | 1 | Lithological differences | 1 |
| 173 | 26.14 | 323 | 207935.1 | 38.76 | 11 | 2 | Lithological differences and close to a fault | 1 |
| 174 | 24.44 | 646 | 190452.1 | 14.31 | 32 | 2 | On the same lithology (TK) | 1 |
| 175 | 20.63 | 1008 | 383598.6 | 26.86 | 11 | 2 | On the same lithology (TK) | 1 |
| 176 | 25.95 | 768 | 314518 | 25.11 | 11 | 2 | On the same lithology (TK) | 1 |

| | | | | | | | | |
|---|---|---|---|---|---|---|---|---|
| 177 | 23.81 | 645 | 194884.1 | 22.28 | 32 | 2 | On the same lithology (TK) | 1 |
| 178 | 20.09 | 1061 | 379381.3 | 10.73 | 11 | 1 | Lithological differences and close to a fault | 1 |
| 179 | 25.38 | 276 | 145037.2 | 52.07 | 30 | 1 | Lithological differences | 1 |
| 180 | 20.07 | 888 | 362310.6 | 26.68 | 11 | 1 | Lithological differences | 1 |
| 181 | 25.32 | 266 | 58985.28 | 10.73 | 39 | 1 | On the same lithology (Tnh) | 1 |
| 182 | 21.12 | 407 | 153734.3 | 19.51 | 30 | 1 | On the same lithology (Tnh) | 1 |
| 183 | 24.58 | 133 | 34618.52 | 10.94 | 39 | 1 | On the same lithology (Tnh) | 1 |
| 184 | 24.46 | 310 | 159225.2 | 591.52 | 32 | 2 | On the same lithology (TK) close to a fault | 1 |
| 185 | 24.07 | 792 | 296115.5 | 15.36 | 11 | 2 | On the same lithology (TK) close to a fault | 1 |
| 186 | 23.79 | 519 | 197332 | 21.87 | 30 | 1 | On the same lithology (Tnh) | 1 |
| 187 | 23.53 | 450 | 259653.4 | 147.47 | 11 | 2 | On the same lithology (TK) close to a fault | 1 |
| 188 | 23.43 | 68 | 31767.64 | 14.16 | 39 | 1 | On the same lithology (Tnh) | 1 |
| 189 | 22.89 | 519 | 264056.3 | 11.9 | 11 | 2 | On the same lithology (TK) | 1 |
| 190 | 23.4 | 327 | 192627.2 | 51.9 | 26 | 2 | On the same lithology (TK) close to a fault | 1 |
| 191 | 23.35 | 235 | 58668.51 | 33.45 | 39 | 1 | On the same lithology (Tnh) | 1 |
| 192 | 23.19 | 1021 | 338792 | 20.16 | 11 | 2 | On the same lithology (TK) close to a fault | 1 |
| 193 | 23.19 | 244 | 141684 | 76.52 | 30 | 1 | Lithological differences | 1 |
| 194 | 23.11 | 90 | 38471.31 | 11.04 | 39 | 1 | On the same lithology (Tnh) | 1 |
| 195 | 22.92 | 224 | 147100.8 | 27.33 | 31 | 1 | Lithological differences | 1 |
| 196 | 22.78 | 235 | 111907 | 39.16 | 36 | 1 | Lithological differences | 1 |
| 197 | 22.66 | 764 | 325176.6 | 10.2 | 11 | 2 | On the same lithology (TK) | 1 |
| 198 | 22.65 | 237 | 135985 | 19.38 | 35 | 1 | On the same lithology (Qt) | 1 |
| 199 | 22.59 | 599 | 232048.8 | 12.51 | 26 | 2 | On the same lithology (TK) | 1 |
| 200 | 22.28 | 273 | 63442.49 | 30.76 | 39 | 1 | On the same lithology (Tnh) | 1 |
| 201 | 21.98 | 332 | 118821.5 | 102.67 | 29 | 1 | On the same lithology (Tnh) | 1 |
| 202 | 21.82 | 864 | 350778.6 | 13.47 | 11 | 1 | Lithological differences | 1 |
| 203 | 21.8 | 338 | 157292.8 | 84.55 | 35 | 2 | On the same lithology (TK) close to a fault | 1 |
| 204 | 21.72 | 311 | 193855.8 | 25.43 | 26 | 2 | On the same lithology (TK) close to a fault | 1 |
| 205 | 21.55 | 269 | 182794.3 | 145.04 | 11 | 1 | On the same lithology (Qt) | 1 |
| 206 | 21.31 | 569 | 294855 | 9.49 | 11 | 2 | On the same lithology (TK) close to a fault | 1 |

| | | | | | | | | |
|---|---|---|---|---|---|---|---|---|
| 207 | 20.67 | 415 | 224091.2 | 23.7 | 11 | 2 | On the same lithology (TK) close to a fault | 1 |
| 208 | 20.59 | 242 | 169371 | 37.85 | 11 | 1 | On the same lithology (Qt) | 1 |
| 209 | 20.33 | 240 | 145747.6 | 29.02 | 32 | 1 | Lithological differences | 1 |
| **Mean** | 37.34 | 813.05 | 275857.8 | 292.95 | | | | |
| **Maximum** | 243.91 | 1786 | 554464.5 | 15179.96 | | | | |
| **Minimum** | 20.02 | 68 | 22264.7 | 8.98 | | | | |